

Response to Referees

We thank the referees for taking the time to assess our manuscript and their useful suggestions for its improvement. Hereafter we answer all the comments.

Anonymous Referee #1

General Comments

The authors present an overview of in-situ measurements of aerosol optical properties made during the DACCIIWA aircraft measurement campaign over the coastal region of Southern West Africa in summer 2016. The region has a varied aerosol environment, in which they sampled mineral dust aerosol, biomass burning aerosol, and anthropogenic pollution. Along with the meteorological situation, instruments on the aircraft measured the aerosol size and vertical distributions, and the aerosol scattering, absorption and extinction coefficients. From this information the authors further derived the aerosol scattering and absorption Ångström exponents, the complex refractive index, the single scattering albedo (SSA), the mass extinction efficiency, and the asymmetry parameter. Using this information, the authors describe the vertical distribution of the aerosols with respect to their optical properties, as well as showing that the SSA of the measured biomass burning aerosols is primarily a function of the imaginary part of the refractive index rather than of the size distribution. The derived SSA values of the biomass burning aerosols appear to be particularly low compared to other measurements from other regions of the world.

This is a very straightforward paper, and I appreciate that the scope of this work is primarily concerned with presenting the measurements and providing an interpretation of their significance. Within this scope, I would say that this is a successful paper, and hence I only have a few minor comments to make.

Specific comments

Figure 1: I assume that the black lines are the flight tracks in background conditions?

Black lines are the tracks of all the flights performed during the field campaign. They include flight tracks in background conditions as well as those in conditions that were not included in our classification due to various reasons (aerosol properties varying during a SLR, instruments not working properly,...).

We have modified Figure 1 to show the selected flight tracks in background conditions. We have also added the location of vertical profiles as requested by Referee #2.

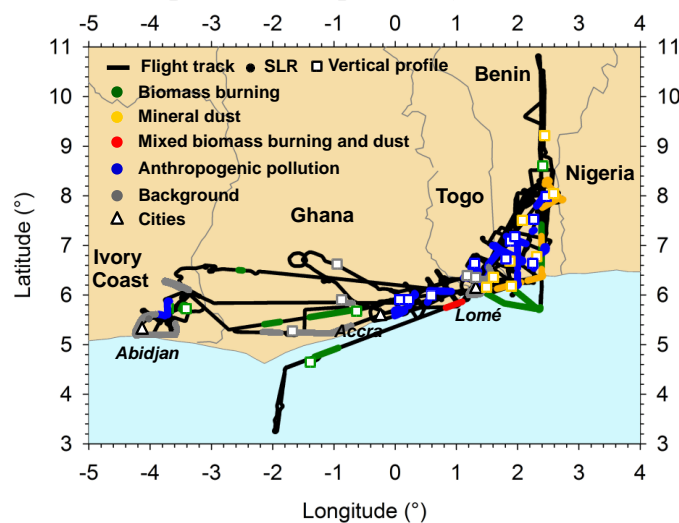


Figure 1. Tracks of the 15 flights analyzed in this study. The colors indicate aircraft flight sampling layers dominated by biomass burning (green), mineral dust (orange), mixed dust-biomass

burning (red), anthropogenic pollution (blue) and background particles (grey) from both vertical profiles (squares) and straight and level runs (SLRs; thick lines).

Section 2.2: as a qualitative comparison, I wonder if it would help to include one of these satellite images (MODIS or SEVIRI) over SWA with one of the flight tracks? This may be useful context to add and may aid the reader's understanding of the regional environment. Maybe such a figure may be more appropriate with respect to Section 2.3.2, and it may also be useful to have an image for each of the aerosol types.

During the summer monsoon, large areas of southern West Africa and Atlantic Ocean are covered by clouds presenting a high surface albedo, making it challenging to observe aerosol properly from satellite observations. When analyzing MODIS or SEVIRI images, we were unable to follow the back-trajectories of dust or biomass burning plumes due to too many cloudy satellite pixels.

Section 2.3.2: might it also be helpful to tabulate (briefly) the aerosol classification specifications? This may be helpful for quick reference when the reader wants to re mind themselves of how the aerosols are classified in the later sections and figures.

The figure below has been added in the paper to illustrate how the aerosols were classified.

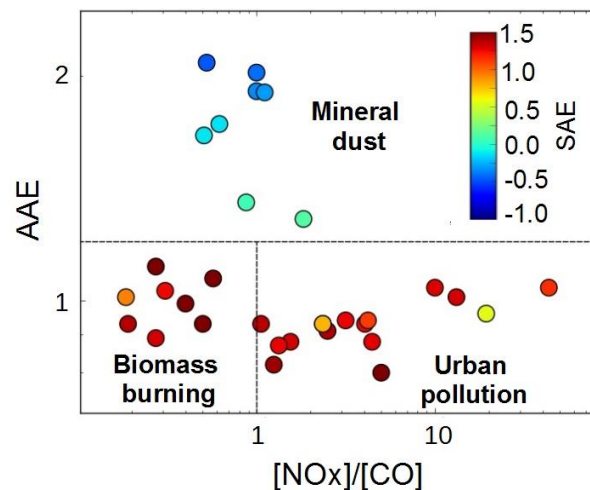


Figure 2. Absorption Ångström Exponent (AAE) as a function of the ratio NO_x to CO. The markers are colored according to the Scattering Ångström Exponent (SAE). Classification of mineral dust, biomass burning and urban pollution particles has been added to the figure.

Figure 5, labels: “wavelength”

Done

Anonymous Referee #2

This paper describes the aerosol physical and optical properties observed during the DACCIWA campaign. The paper is based on in-situ measurements performed a-board the ATR-42. The paper is well written and the topic fits the ACP's scope. However, I have many remarks and some needs to be taken into account before this paper could be published in ACP.

Major comments

The title of this manuscript. I believe the title refers to the BB aerosols that were observed with really low SSA in comparison to all previous results. However, this part is described only on the 23th page. I would strongly recommend changing it to "aerosol optical properties overview during the DACCIWA campaign" or something similar.

The title has been changed to: *“Overview of aerosol optical properties over southern West Africa from DACCIWA aircraft measurements”*

First major comments about the Mie code used for this study. So you stated few lines (P8 L237-245) about how you used the Mie code to retrieve the refractive index of aerosols (reverse method) based on their physical and optical properties. First of all you are using a Mie code for dust and BB aerosols. In fact you measure the asymmetry factor (which is not that good with the TSI nephelometer) and found out that the particles are far from spherical. You never stated the possible issues with it. Then you never say a word for the mixing state you used. I found a word about it later when you say that the mixing was external which was consistent with previous observations. Have you tested the case with internal mixing (either core shell or just coating) ? Moreover, what is the acceptable difference between measurements and calculation to stop the iterative process (5%, 10% more ???)? Is it just iterative process with an a priori k and n or it an optimal estimation method that will avoid any local minimum? Later on (P20-21, L548-556), you used the Mie code again but this time I believe not in a reverse mode. So you entered a k and n along with the size distribution and you get optical properties that you used to calculate a SSA. Which k and did you used? In Africa, there are many sources of dust and BB aerosols associated with many different k and n... How these calculations made with a Mie code, for spherical particles, prove that your aerosols are externally mixed? You need here to prove it with a spheroidal code, for different mixing state.

We have chosen to use a Mie code to calculate the aerosol optical parameters by assuming the particles are spherical. First, because the particle shape was not measured during the field campaign and it would be very hazardous to associate a shape to the aerosols, especially since aerosols from different sources were sampled at different times after emission. Second, this facilitates a quantitative comparison with past data, since a large majority of them used this simplification. Third, because climate models usually use Mie theory due its computational efficiency and applicability to radiative transfer models.

To explain this choice we added the following text in Section 2.3.1: *“Optical calculations were performed using Mie theory, implying a sphericity assumption, because it facilitates a quantitative comparison with past data, mostly using this simplification and because most climate models assume spherical properties.”*

Concerning the aerosol mixing state, the application of Mie theory in our retrieval procedure to calculate aerosol optical parameters requires information about the size distribution, refractive index and particle density. These input parameters refer to the properties of the overall particle population within the aerosol. There is no assumption in the aerosol mixing state. By contrast, in climate models, the aerosol optical parameters are calculated from multiple particle types with

different chemical composition and apply a mixing rule to calculate the refractive index of the aerosol from the refractive indices of the individual component species. Therefore, the mixing state of the aerosol must be addressed for climate modelling to calculate aerosol radiative forcing. Currently, the most common assumption made in climate models, which is also the easiest from a computational perspective, is that the aerosols are externally mixed. This is the reason why we assessed whether the assumption of external mixing allow to reproduce the observed optical properties in section 4.1. To test internal mixing assumption would need to know to what degree the aerosol population is internally-mixed. In fact, there are an enormous number of degrees of freedom in the aerosol mixing state. Even within a single distribution mode there are a prohibitively large number of combinations involved in mixing the constituents. At one extreme the aerosols can be internally mixed as a homogeneous material reflecting the chemical and physical average of all the contributing components. At another extreme, each aerosol component is physically separated from the other components creating an external mixture of chemically pure modes. The real mixing state can be expected to lie somewhere in between these two extremes, with aerosol in an external mode that is or is not an internal mixture of components. Therefore, in the absence of information on mixing state and chemical composition of individual particles, we cannot test internal mixing assumption.

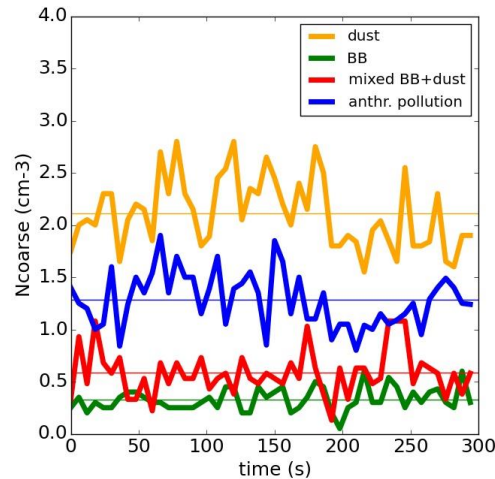
We have added more information in the paper about the choice of the refractive indices used in the Mie code in section 4.1: *“The refractive indices at 550 nm were assumed to be 1.52-0.002i and 1.60-0.040i for dust and anthropogenic pollution particles, respectively, which are the mean values deduced from the data inversion procedure.”*

We have also added more information about the iterative process developed to calculate aerosol optical parameters in section 2.3.1: *“The retrieval algorithm consists of iteratively varying the real part of the complex refractive index (m) from 1.33 to 1.60 and the imaginary part of the complex refractive index (k) from 0.000 to 0.080 in steps of resolution of 0.001. m and k were fixed when the difference between calculated values of σ_{scat} and σ_{abs} and measurements was below 1%.”*

Number concentration of coarse particles. The authors are showing number concentrations of particles from 1-5 μ m. These concentrations are measured from the OPC-GRIMM. The concentrations are between 0 and 2.5 cm^{-3} . Could you provide the reader the noise of this instrument regarding these large particles. Is it significant ?

The advantages of an OPC is that (1) it can count particle numbers very accurately when the concentration is low; (2) it has very good signal to noise ratios for large particles (>1 μ m). The figure below shows the time evolution of particle concentration from 1-5 μ m measured by the OPC-GRIMM for different aerosol plumes sampled during straight levelled runs. You can see that the signal to noise ratio was higher than 3 for all the aerosol plumes, which make the instrument well suited to quantify particle concentration in this size range.

We have added this information in section 2.3.1.: *“The signal to noise ratio of the OPC for particles in this size range was higher than 3, which makes the instrument well suited to quantify variations in N_{coarse} .”*



Temporal variation of particle number concentration measured in the size ranged 1-5 μ m by the GRIMM-OPC during different SLRs.

During the field campaign, the ATR-42 performed vertical profiles at the beginning of each flight. These are used in Figure 3. On Figure 1, you highlighted the BB, dust and pollution plumes. How far are the vertical profiles from the plume observed? I wonder how the variability of the vertical profile average is due to the distance to the actual plume. I had to wait until Figure 6 (P21) to have information about altitudes at which you observed the different plumes. At P14 L366-370, P15 L398-399, you are showing that aerosols, within a layer located below 2.5km, are efficiently mixed with anthropogenic emissions. Then on Figure 6 you are trying to interpret the optical variations throughout the vertical profile. From my understanding, if you are interested in “pure” BB or Dust particles than you should only show/interpret vertical profiles from 2.5km up to 4km.

The location of vertical profiles has been added in Figure 1. You can see that the vertical profiles were located near the straight leveled runs.

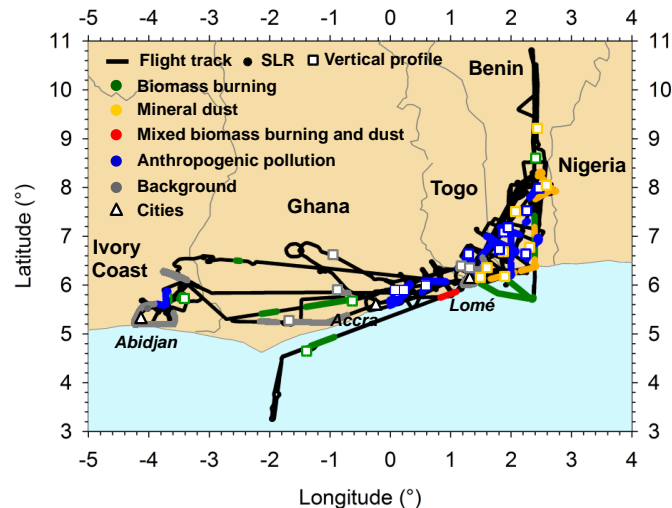


Figure 1. Tracks of the 15 flights analyzed in this study. The colors indicate aircraft flight sampling layers dominated by biomass burning (green), mineral dust (orange), mixed dust-biomass burning (red), anthropogenic pollution (blue) and background particles (grey) from both vertical profiles (squares) and straight and level runs (SLRs; thick lines).

Data presented in Figure 6 (now Figure 7 in the update manuscript) are based on measurements during SLR. This has been clarified in the paper at the beginning of section 4.1.: “We exclusively

consider measurements acquired during SLRs, since only during these phases the whole set of aerosol optical properties were measured.”

Minor remarks

Page 2 L37 : I think something is missing to introduce properly the BB aerosols or just to skip a line here.

The sentence has been rewritten as follows: “For the layers dominated by the biomass burning particles, aerosol particles were significantly more light absorbing than those previously measured in other areas (e.g. Amazonia, North America) with SSA ranging from 0.71 to 0.77 at 550 nm.”

Page 2 L68 : It’s usually called MEE that stands for Mass Extinction Efficiency and its units is m^2/g not g/cm^3 . In the table2’s caption you even called it extinction mass efficiency. Please be consistent throughout the manuscript. By the way how did you measure the mass concentration of aerosols ? Did you assume a density for each type ? And did you assume the same density for each mode ?

We have changed MEC by MEE in the text.

Information about the mass densities of each aerosol type used to calculate aerosol mass concentration and henceforth MEC are already provided on P8 in L261-264.

P3 L73-75: Why do you introduce remote sensing data that you will never ever talk again ?

Our intention is to provide a comprehensive overview of aerosol optical properties over SWA for the climate modelling and the remote sensing communities. From the remote sensing perspective, in-situ data constitutes independent verification of satellite data products and can be used to assess the performance of inversion algorithms. For known TOA reflectance, the retrieval of AOD is very sensitive to aerosol size distribution and refractive index. Improper assumptions used in the algorithm regarding such key parameters may lead to a spurious AOD long-term trend in the regions under influence of absorbing particles due to the regional biases. This is the reason why we introduce remote sensing measurements in the introduction and we invite the remote sensing community to use this dataset in the conclusion.

P3 L112 remove the ‘s’ at aerosol

Done

P 5 When DACCIWA took place (month, year) ? What season was it (apparently during the monsoon period)?

The campaign period is already presented before on P4.

P6 L 176 : the CPC MARIE model needs to be described here. There is no paper associated with this instrument and I was unable to find any specifications on internet. Is it working with a flow regulator or a critical orifice? How is it counting in comparison to any TSI CPC ? You used the CPC measurements to infer the N_{fine} but you never say anything about a comparison, in term of number concentration, with the OPC, UHSAS or the SMPS. As this instrument is not (yet?) considered as a reference, you cannot use it like a reference. You could use the calibration data for the size distribution (PSL and oil) to prove that this instrument was measuring the same number concentrations than the OPC.

The international standard method defined by the European Committee for Standardization for determining the particle number concentration is based on a CPC (CEN/TS 16976:2016). This instrument is considered as a reference for ambient aerosol monitoring for many years. The CPC Marie allows measuring number concentration of particle with a size above 10-15 nm

(depending on the temperature conditions). It is structurally the same as a TSI CPC3010 except that there are more controls on the condensation and saturator temperatures and thermal dissipation has been improved. Thus, its measurement behavior is comparable to a TSI CPC3010 (Mertes, Schröder, and Wiedensohler, 1995; Russell et al., 1996; Wiedensohler et al., 1997). OPC, UHSAS and SMPS are measuring particle size distribution in limited size ranges (0.3-32 μm for OPC, 0.1-1 μm for UHSAS during DACCIWA, 0.02-0.5 μm for SMPS). Given the relative importance of the smallest particles to the total concentration, the CPC concentration can be considered as the best estimation of the total particle concentration sampled.

We have added in the text the following references that provide a description and validation of the CPC Marie, as well as its intercomparison with other CPCs: *Mertes, Schröder, and Wiedensohler, 1995; Russell et al., 1996; Wiedensohler et al., 1997.*

Concerning the calibration experiment suggested by Referee #2, artificially produced PSL (or oil) particles would generate a mixture of air/water/PSL(oil) mixture with elevated concentration of ultrafine particles. These small particles cannot be fully detected by the OPC, UHSAS or SMPS instruments, so direct comparisons between instruments won't be relevant for this experiment. Otherwise, Marie CPC and SMPS CPC have been inter-compared in the laboratory at low pressure with concentration differences lower than 10%.

P6 L 187 Replace 525 by 550nm.

Done

P10 section 2.3.2: A figure showing the AAE versus the SAE would have been appreciated here.

The new figure below has been added in the paper.

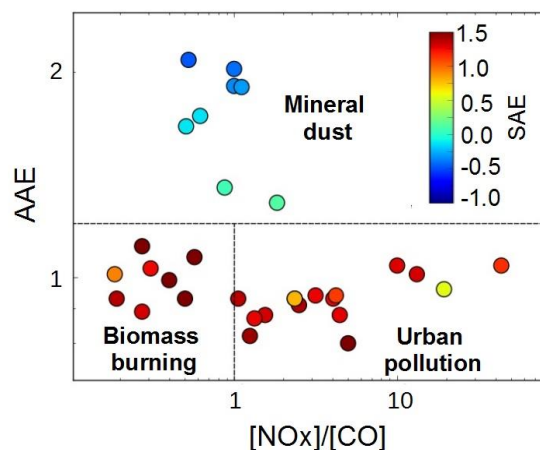


Figure 2. Absorption Ångström Exponent (AAE) as a function of the ratio NO_x to CO. The markers are colored according to the Scattering Ångström Exponent (SAE). Classification of mineral dust, biomass burning and urban pollution particles has been added to the figure.

P10 L282 : remove the 's' at the end of theses

Done

P11 L 301 : I believe that the background is also without the detectable influence of Dust and BB as well as anthropogenic emissions.

Done

P13 L334: The AEJ is a synoptic flow. It is always present over West Africa at a specific location (between 10-20 °N between 2-6km). The ATR flew between 3-11°N. Therefore, I don't see how you would have been able to observe it and why you would have been able to observe it for specific cases and not for the others.

The average climatological position of the AEJ varies during the summer between 10°N in June and 15°N in July. However, because it is a synoptic feature, the position of the AEJ core varies significantly from day to day, the DACCIWA period being no exception as shown by Knippertz et al., 2017 using ERA-I reanalysis data. In their Figure 8, Knippertz et al. (2017) show that the position of the AEJ on 2 July is centered at 4°N and on 10 July at 24°N. This is due to the many disturbances sweeping through southern West Africa during the monsoon season, which impact the location and the intensity of the AEJ core.

It is also worth pointing out the AEJ is a broad feature, generally confined to a width of 5°–10° of latitude as seen in reanalyses, but also in the airborne observations made using dropsondes along north-south transects across southern West Africa during JET 2000 (Tompkins et al., 2005) and AMMA in 2006 (Flamant et al., 2009). In the later study, the southern fringe of the AEJ is observed to reach the latitude of the SWA coast around mid-July.

Therefore, due to the important day to day variability of its mean position, but also of this latitudinal width, we can assess that observations made with the ATR between 3–11°N were indeed acquired in regions impacted by the AEJ and under a variety of AEJ-forcing conditions.

We have added a sentence about the latitudinal variation of the AEJ: *“Above 2.5 km amsl, the wind speed increases in the urban pollution and dust cases and the wind remains easterly, indicating the presence of the African easterly jet with its core typically farther north over the Sahel (Figure 8 in Knippertz et al., 2017 for the latitudinal variations of the African easterly jet during the DACCIWA field phase).”*

P13 L 335 : there are two dots after Sahel.

Done

P13 L356-357 : According to the Nfine vertical profile, the BB plume is observed from 2.5 – 4km. Your sentence isn't clear for me. Is this between the surface up to 4km or as suggested by the Nfine vertical profile ?

We have clarified in the paper that we refer to the BB plumes transported above 1.5 km asl: *“The biomass burning plume extends from 1.5 to 5 km amsl and is associated with transport from the southwest in a layer of enhanced wind speed just below 4 km amsl as discussed above.”*

Figure 4 : I think you could do something in this figure to show the altitude of each SLR. You never mentioned that the different lines in Figure 4b were associated to all the plumes observed. Maybe the line width of each line could be coded as a function of the altitude? Obviously for dust plume one SD is significantly different from the others. Why ?

We have modified the figure to show the altitude of the aerosol sampled.

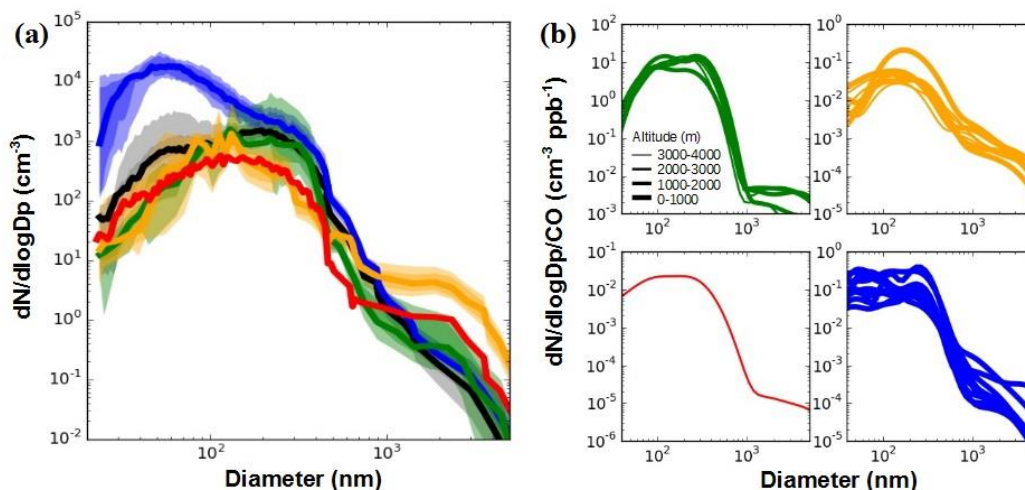


Figure 5. (a) Statistical analysis of number size distributions with colored areas representing the 3th, 25th, 75th and 97th percentiles of the data and (b) number size distributions normalized to CO for plumes dominated by biomass burning (green), dust (orange), mixed dust-biomass burning (red), anthropogenic pollution (blue) and background particles (black). In panel b, the line thickness is scaled by the altitude of the aerosol plume.

P15 L 388 : remove ‘the’ in front of plumes

Done

P15 L 392-393 : This is impossible to see that on Figure 4. We could see something on Figure 4b but it could also be result of the CO concentration...

Colors in the figure have been changed to enable a better observation of variability in particle concentration (see figure above).

L 395 – 396 : We must trust you about the fact that the smaller particles are observed within the lower dust plume...

We have added in the text that this observation can be seen in the previous Figure 3.

P 15 L 401-406: Again you stated that below 2.5 km all the aerosol are mixed. You observed 3 dust plumes below 3km. I assume that these three samples where associated with the small particles. The BB plumes where observed above ~2.2km. I’m not convinced that the location has anything to do but mainly the altitude... Most of the BB plumes have been observed close to big cities (Abidjan, Accra, Lome).

As written in the paragraph, BB and dust plumes were sampled at approximatively the same altitude. The lowest BB plumes was observed at 2.2 km asl., which do not make a big difference with the dust plume sampled at 2.0 km asl. Since pollution plumes were exported up to 2.5 km asl., the altitude is probably not the reason of the different mixing with pollution plumes.

P15 L417-419 : The accumulation mode exceeds the amount of large particle. What is “large particle” here ? As there are no information about the mode the authors are referring to, it’s hard to follow. There is probably a need for a table that describe all the modes observed for each aerosol type. Anyway, is that surprising in number concentration?

“Larger particles” has been replaced by “particles centered at 230 nm” in the text for clarity.

It is already explained in the paragraph that the mode centered at 100 nm is surprising for aged biomass burning, when comparing with the literature.

P16 L 423. In this part you are talking about a phenomenon observed by colleagues during two specific days. Do they observe it during other days ? Could it happen during other days ? As you are not explaining the general mechanism there is no way for us to infer if this could have happen during the whole campaign. So when did you observed all plumes ? Was it during these specific days ? If not how do you know that this is always the case between the surface and 2.5km ?

We have removed the sentence referring to papers of Flamant et al. (2018) and Deroubaix et al. (2019).

P16 L430 : So the same dusty mode was observed during several campaigns over West Africa. From this observation you conclude that dust does not efficiently mix with other particles. Could you please explain ?

The coarse mode of the dust plume is expected to be impacted by the mixing with other particles in case of an internal mixing, which should somewhat increase the particle size. We have clarified it in the manuscript: “The super-micron mode of the dust plume is expected to be impacted by the mixing with other particles in case of an internal mixing, which should somewhat increase the particle size”.

P16 L435: Then, within the anthropogenic pollution plumes you observed a coarse mode. As the sites are nearby the coast you assume that it could be sea salt. Do you have any evidence for that? Could it be dust or road dust or pollens or any other large particles???

Analysis of the spectral dependence of aerosol optical properties allows for interpretation of aerosol chemical composition. As stated in sections 2.3.1 and 2.3.2, mineral dust particles have the unique ability to absorb light strongly in the blue to ultraviolet spectrum. The presence of dust particles in aerosol plumes is thus expected to increase AAE above 1. We measured AAE in the range 0.7-1 in anthropogenic pollution plumes, which suggests negligible contribution of mineral dust in these plumes. This result is not surprising since anthropogenic pollution plumes originated from the south while the source region of dust was located in the north east when looking at the backtrajectories of air masses (Figure 2). For anthropogenic pollution plumes being sampled near the coast and below 0.5 km amsl, mixing of sea salt in pollution plumes is the most relevant interpretation for the presence of a coarse mode.

We have added the following explanation in the manuscript: “We measured AAE in the range 0.7-1 in anthropogenic pollution plumes (Figure 2), which suggests negligible contribution of mineral dust in these plumes. This coarse mode has most likely significant contributions from sea salt particles, as plumes arriving from the cities were transported at low altitude over the ocean (Fig. 3).”

P17 L458 : The strongest spectral dependence of SSA is observed for the lowest absorption plume. Well from the Figure 5b this is not the case. Indeed, the largest SSA values for the BB aerosol at 440nm (Around 0.78) show a quite strong SSA at 660nm (around 0.74) and therefore quite a low spectral dependencies. The largest spectral depend are observed for both ‘middle’ SSA values at 440nm. Could you then remove the part right after that suggest similar results with the literature that are no more consistent with your results?

The referee is right. We have removed this part.

P18 L477 : I found it really odd for you to compare small SSA spectral dependencies observed over African cities using in-situ measurements with literature using AERONET measurements or even with plumes observed over European cities. The principle (column integrated versus in situ) of measurements as well as the pollutants (European polluted plumes are clearly different from African polluted plumes) have to be a bit similar to gain information. In this case arguing that what you observed is entirely different from these studies is not convincing.

AERONET has been extensively compared with various types of airborne in situ airborne measurements for a range of different aerosol types including urban pollution particles and the Africa continent. These were recently summarized in Andrews et al. (2017). They confirm previously reported comparison that the large majority of SSA comparisons for AOD > 0.2 are within the reported in-situ SSA uncertainty bounds, while AERONET inversions tend to overestimate SSA for low AOD. All AERONET measurements that included the AOD > 0.2 constraint have shown that SSA systematically decrease with increasing wavelength for a range of different urban pollution plumes across the world (Dubovick et al., 2002; Shin et al., 2019). However, in the light that no AERONET or in-situ measurements are available for comparison in other African cities, we have nuanced the sentence: “However, the flat spectral dependence of SSA appears to be anomalous for anthropogenic pollution aerosols, as SSA has been shown to decrease with increasing wavelength for a range of different urban pollution plumes over European, American and Asian cities (Dubovick et al., 2002; Di Biagio et al., 2016; Shin et al., 2019).”

P18 L 481 : During the NAMMA campaign, Omar et al. compare the extinction coefficients from the LIDAR and from the in situ measurements (assuming a dust LIDAR ratio). They found that the extinction was really close and then that no large aerosol was lost within the inlet. I'm sure you could do something similar here to estimate the losses for all cases.

This paragraph was unclear. We wanted to highlight the difficulty to compare our results with previous measurements because the measurement of SSA is highly dependent on the extent to which the coarse mode is measured behind the aerosol sampling inlet. For instance, Ryder et al. (2013) found an overestimation of SSA in dust plumes when the SSA is measured behind inlet during the FENNEC campaign. In our case, the impact of the Community Aerosol Inlet on the measured optical properties has been calculated for dust aerosols in Denjean et al. (2016). We found that the absolute error associated with SSA, g and MEE due to the aircraft inlet is in the range covered by the measurement uncertainties. However, different aerosol inlet systems were used during previous field campaigns (cut-off diameter of 5µm during DACCIWA and 2.5µm for Weinzierl et al. (2011) during SAMUM-2 for instance), which can lead to discrepancies when comparing SSA from different campaigns.

The paragraph has been changed as follows: “The magnitude of SSA increased at the three wavelengths when dust events occurred. Large variations in SSA were obtained with values ranging from 0.76–0.92 at 440 nm, 0.81–0.94 at 550 nm and 0.81–0.97 at 660 nm. The measurement of SSA is highly dependent on the extent to which the coarse mode is measured behind the aerosol sampling inlet. Denjean et al. (2016) found that the absolute error associated with SSA, g and MEE of dust aerosols due to the CAI inlet is in the range covered by the measurement uncertainties. However, different aerosol inlet systems were used during previous field campaign, which makes comparison of our results with previous measurements difficult.”

P18 L484 : ‘measurements are comparable to each other’. So I'd like to disagree with you. It depends on the event right ? Some events will be associated with uplifting of large particles and therefore the

inlet cut off may play a major role OR some events could also be associated with uplifting of smaller particles and then the inlet cut-off won't be an issue anymore.

As explained in the previous comment, the paragraph was unclear and has been rewritten.

P19 clarify MEE versus MEC vs extinction mass efficiency vs extinction mass coefficient!

We have exchanged MEC by MEE in the text.

P19: Another Mie test... So now you used a Mie code to estimate the impact of each aerosol mode ? Could you please explain what you did and how you did it ? We found MEC to be positively correlated with SAE (not shown) with measurement wavelengths (450–660 nm), which agrees with Mie theory. Again, I don't understand the sentence. Are you talking about measured MEE vs measured SAE having the same correlation than the calculated one ? What about a straight comparison of SAE/MEE calculated and observed ? And how this correlation is relevant for your analysis ?

This is not another Mie test; this is the result of the iterative process that provides SSA, MEE and g. The aim of the sentence is to explain some of the variability in MEE for a given aerosol type. SAE being a good proxy for variation of size distribution for a given aerosol chemical composition, it was expected that MEE correlates with SAE.

To clarify this, we have rewritten the sentences as follows: “MEE is heavily influenced by the mass concentrations in the accumulation mode where the aerosol is optically more efficient in extinguishing radiation. We found MEE to be positively correlated with SAE (not shown), which was expected because of the dependence of MEE on particle size”.

P19 L 509-511: So the total and back-scattering coefficients have an error associated with the measurement principle. Did you correct the data following Anderson and Ogren recommendations? What are the error associated with the measurements and then with the g calculation? Moreover, the g is also affected by the morphology of the particle.

Data were corrected for truncation error using a Mie code in the data inversion procedure that takes into account the aerosol size distribution. This correction is more accurate than the Anderson and Ogren recommendations which are based on single sample. This was already written in Table 1 and Appendix 2, but we have added the following sentence in section 2.1. : “The particle scattering coefficients (σ_{scat}) at 450, 550 and 635 nm were measured using a AURORA3000 3-wavelength nephelometer and corrected for angular truncator error in the data inversion procedure using a Mie code (i.e. Section 2.3.1 and Appendix 2).”

Concerning the aerosol morphology, please look at our response above in major comments.

P20: Is this part 4 based on single SLR analysis ?

Yes, it is now specified in the text: “We exclusively consider measurements acquired during SLRs, since only during these phases the whole set of aerosol optical properties were measured.”

P20 L530 – 532 : On figure 6c there are no dots below 1500m and I cannot see the NO_x decrease that you are talking about.

The sentence has been removed.

P20 L 532 : You qualify it as a strong SSA variation (0.8 to 0.95) but since page 15 you told us that below 2.5km all the layers are mixed together. From the number concentration profile there are almost no dust at that altitude (below 1cm-3).

We clearly mentioned previously that large variations in the concentration of fine particles (sections 3.1 and 3.2) and SSA (section 3.3) were observed in dust plumes. Concerning the concentration, only small number concentration of dust particles will contribute significantly to the aerosol mass concentration and extinction coefficient, and consequently to the aerosol radiative effect. You can see that effect in Fig 3a, which shows that the extinction coefficient increased from 20 to 80 Mm^{-1} when dust was transported at 2.5 km asl over the region.

P21 L564 : An Figure 6 indicates markedly different processes affecting optical properties of biomass burning aerosols. Az Which processes are highlighted by this figure ? To me, all BB profiles on Figure 6 are notably stable.

The sentence has been removed.

P21 L569 : An remote location Az . Please define it. For me the anthropogenic plumes were also observed in remote location, don't you think ?

We have removed the part of the sentence about the location of BB.

P21 L564 to P22 L 578 : I don't really understand the need for this paragraph. There are no new information and we also have to wait for further explanations.

The important message of this paragraph is that BB plumes were not affected by pollution emissions. This interpretation is based on Fig. 6 showing the vertical distribution of SSA, SAE and NO_x concentrations. So we think it is very important to keep this discussion here. However, we agree that the end of the paragraph can be moved in section 4.2 and it has been done.

P22 L589 – 591 An We did not find any correlation between the values of SSA and their spectral dependence, which suggests that the variability in SSA cannot be attributed to different contributions of marine aerosol in pollution plumes. Az So I'm not sure I do understand this statement. A correlation between SSA values and their spectral dependency is evidence that SS are not contributing much?

We have removed this sentence.

P22 L595 – 597 “The high absorbing properties ($SSA \approx 0.81$ at 550nm) of background aerosols is consistent with being a mixture of aged biomass burning and Atlantic marine aerosol. Az Please explain. And An Moreover SSA of background aerosol was lower than previously reported over the Southern Atlantic (Ascension Island) outside the fire season in Central Africa (Zuidema al., 2018), which supports this conclusion. Az Now I'm missing something. You are comparing measurements performed over a small island, far from any anthropogenic sources or any natural sources of absorbing particles, to your results and found that aerosols you observed are more absorbing. Is that surprising at all ? Does that prove that you observed BB aerosols or rather anthropogenic aerosols ?

Concerning the interpretation of the low SSA in background plumes, we have completed the sentence as follows: “The high absorbing properties ($SSA \approx 0.81$ at 550nm) and the presence of particles both in the accumulation and super-micron modes (i.e. section 3.2.) in background plumes are consistent with being a mixture of aged absorbing biomass burning and Atlantic marine aerosol.”

We have removed the sentence comparing our measurements with those of Zuidema et al. (2018), since it is discussed in more details in the next section.

P22 L207 : A variation of SAE could be due to a size shift if you know that chemical composition, mixing state and morphology are similar. In this case you don't show any chemical results but you have the SD. Why using SAE to highlight the size variation ?

As mentioned in section 2.3.1., the value of SAE depends primarily on the size of the particles, such that small values of SAE indicate larger aerosol particle, and large values of SAE indicate relatively smaller aerosol. This parameter is widely used in the community for studying the variability in aerosol size distribution because it is a sensitive parameter that needs limited corrections (only the truncation of the nephelometer). Using the measured aerosol size distribution would bring a higher degree of uncertainty due to the need to correct measurements with the aerosol refractive index.

L 611-613 Could you be more precise with the reference you cited ? Where were this studies perform and what were the particle diameter at the formation and after few hours ?

We have completed the sentence as follows: “with previous observations of size distribution in aged North American biomass burning plumes”. The range of particle diameter reported in these studies was already provided section 3.2.

P23 L622 : An by the variability in composition of biomass burning aerosol Az Please add a ref that prove that k is only linked with the aerosol chemical composition. Could you also show the spectral dependency of k ?

k is not only linked with the aerosol chemical composition, it also depends on the size distribution of the particle species. However, given that SSA was previously found to be independent of the aerosol size distribution (Figure 8a), Figure 8b suggests that SSA variability was strongly influenced by the variability in composition of biomass burning aerosol. The paragraph has been rewritten as follows: “In contrast, Figure 8b shows that there was a consistent decrease in SSA with increasing k, although there is some variability between the results from different plumes. The observed variability of SSA is reflected in a large variability of k, which is estimated to span the large range 0.048–0.080 at 550 nm. k depends both on the aerosol chemical composition and size distribution (Mita and Isono, 1980). Given that SSA was found to be independent of the aerosol size distribution (Figure 8a), Figure 8b suggests that SSA variability was strongly influenced by the variability in composition of biomass burning aerosol, implying a high contribution for light-absorbing particles.”

P25 L699 : You need to prove using chemical composition data that BB were not affected by the mixing with anthropogenic emissions (at least for the lowest SLR).

This has been intensively discussed in section 4.1 by looking at the vertical variability of SSA, SAE and NOx concentration. It was also discussed in section 3.2 with the analysis of aerosol size distribution in BB plumes.

P26 L717 : You never show the background SSA spectral dependency.

It is already shown Fig. 5 (a) in grey.

P26 L 721 : An The large proportion of aerosols emitted from cities that resided in the ultrafine mode particles” Are you talking about African Cities or any city in general ? Do you have a reference? From your observations, you always have the background aerosol mixed with the city plume, right ? So you cannot tell what is coming from cities and what is coming from the background, right ? Or you made a difference between both SD ?

The interpretation of the ultrafine mode has been already intensively discussed in section 3.2. As stated in the text, this mode is only observed in plumes originating from the polluted cities of Lomé, Accra and Abidjan.

In the conclusion, we have clarified the origin of the anthropogenic aerosols: “The large proportion of aerosols emitted from the cities of Lomé, Accra and Abidjan that resided in the ultrafine mode particles have limited impact on already elevated amounts of accumulation mode particles having a maximal absorption efficiency”.

The appendixes need to be called in the main text.

Appendixes were already called in the text (P5 for Appendix 1 and P7 for Appendix 2).

References :

Andrews, E., Ogren, J. A., Kinne, S., and Samset, B.: Comparison of AOD, AAOD and column single scattering albedo from AERONET retrievals and in situ profiling measurements, Atmos. Chem. Phys., 17, 6041–6072, <https://doi.org/10.5194/acp-17-6041-2017>, 2017.

Flamant, C., C. Lavaysse, M. Todd, J.-P. Chaboureau and J. Pelon, 2009: Multi-platform observations of a springtime case of Bodélé and Sudan dust emission, transport and scavenging over West Africa, Q. J. Roy. Meteorol. Soc., 135, 413-430.

Mita, A., Isono, K.: Effective complex refractive index of atmospheric aerosols containing absorbing substances, J. Meteorol. Soc. Jpn., 58, 69-80, https://doi.org/10.2151/jmsj1965.58.1_69 1980.

Mertes, S., Schröder, F., Wiedensohler, A.: The particle detection efficiency curve of the TSI 3010 CPC as a function of the temperature difference between saturator and condenser, Aerosol Science and Technology, 23, pp. 257-261, 1995.

Russell M., Zhang, S.-H., Flagan, R.C., Seinfeld, J.H., Stolzenburg, M.R., Caldow, R.: Radially classified aerosol detector for aircraft-based submicron aerosol measurements, Journal of Atmospheric and Oceanic Technology, 13, 598-609, 1996.

Ryder, C. L., Highwood, E. J., Rosenberg, P. D., Trembath, J., Brooke, J. K., Bart, M., Dean, A., Crosier, J., Dorsey, J., Brindley, H., Banks, J., Marsham, J. H., McQuaid, J. B., Sodemann, H., and Washington, R.: Optical properties of Saharan dust aerosol and contribution from the coarse mode as measured during the Fennec 2011 aircraft campaign, Atmos. Chem. Phys., 13, 303–325, <https://doi.org/10.5194/acp-13-303-2013>, 2013.

Shin, S.-K., Tesche, M., Noh, Y., and Müller, D.: Aerosol-type classification based on AERONET version 3 inversion products, Atmos. Meas. Tech., 12, 3789–3803, <https://doi.org/10.5194/amt-12-3789-2019>, 2019.

Tompkins A., M., A. Diongue-Niang, D. J. Parker, C. D. Throncroft, 2005 : The African easterly jet in the ECMWF Integrated Forecast System: 4D-Var analysis, Q. J. R. Meteorol. Soc. (2005), 131, pp. 2861–2885 doi: 10.1256/qj.04.136.

Wiedensohler, A., Orsini, D., Covert, D.S., Coffmann, D., Cantrell, W., Havlicek, M., Brechtel, F.J., Russell, L.M., Weber, R.J., Gras, J., Hudson, J.G., Litchy M.: Intercomparison study of size-dependent counting efficiency of 26 condensation particle counters, Aerosol Science and Technology, 27, 224-242, 1997.

1 **Overview of aerosol optical properties over southern**
2 **West Africa from DACCIWA aircraft measurements**
3 ~~**Light absorption properties of aerosols over Southern**~~
4 ~~**West Africa**~~

5
6 Cyrielle Denjean¹, Thierry Bourriane¹, Frederic Burnet¹, Marc Mallet¹, Nicolas
7 Maury¹, Aurélie Colomb², Pamela Dominutti^{2,*}, Joel Brito^{2,**}, Régis Dupuy²,
8 Karine Sellegri², Alfons Schwarzenboeck², Cyrille Flamant³, Peter Knippertz⁴

9
10 ¹CNRM, Université de Toulouse, Météo-France, CNRS, Toulouse, France

11 ²LaMP, Université de Clermont Auvergne, Clermont-Ferrand, France

12 ³LATMOS/IPSL, Sorbonne Université, UVSQ, CNRS, Paris, France

13 ⁴Institute of Meteorology and Climate Research, Karlsruhe Institute of Technology,
14 Karlsruhe, Germany

15 * Now at Wolfson Atmospheric Chemistry Laboratories, Department of Chemistry,
16 University of York, YO10 5DD- York, UK

17 ** Now at: IMT Lille Douai, Université de Lille, SAGE, Lille, France

18
19 *Correspondence to : Cyrielle Denjean (cyrielle.denjean@meteo.fr)*

20
21 **Abstract.** Southern West Africa (SWA) is an African pollution hotspot but a relatively poorly
22 sampled region of the world. We present an overview of *in-situ* aerosol optical measurements
23 collected over SWA in June and July 2016 as part as the DACCIWA (Dynamics-Aerosol-
24 Chemistry-Clouds Interactions in West Africa) airborne campaign. The aircraft sampled a wide
25 range of air masses, including anthropogenic pollution plumes emitted from the coastal cities,
26 long-range transported biomass burning plumes from Central and Southern Africa and dust plumes
27 from the Sahara and Sahel region, as well as mixtures of these plumes. The specific objective of
28 this work is to characterize the regional variability of the vertical distribution of aerosol particles
29 and their spectral optical properties (single scattering albedo: *SSA*, asymmetry parameter,
30 extinction mass efficiency, scattering Ångström exponent and absorption Ångström exponent:
31 *AAE*). First findings indicate that aerosol optical properties in the planetary boundary layer were
32 dominated by a widespread and persistent biomass burning loading from the Southern
33 Hemisphere. Despite a strong increase of aerosol number concentration in air masses downwind of
34 urban conglomerations, spectral *SSA* were comparable to the background and showed signatures of

35 the absorption characteristics of biomass burning aerosols. In the free troposphere, moderately to
36 strongly absorbing aerosol layers, dominated by either dust or biomass burning particles, occurred
37 occasionally. In aerosol layers dominated by mineral dust particles, *SSA* varied from 0.81 to 0.92 at
38 550 nm depending on the variable proportion of anthropogenic pollution particles externally mixed
39 with the dust. **For the layers dominated by biomass burning particles, aerosol particles** were
40 significantly more light absorbing than those previously measured in other areas (e.g. Amazonia,
41 North America) with *SSA* ranging from 0.71 to 0.77 at 550 nm. The variability of *SSA* was mainly
42 controlled by variations in aerosol composition rather than in aerosol size distribution.
43 Correspondingly, values of *AAE* ranged from 0.9 to 1.1, suggesting that lens-coated black carbon
44 particles were the dominant absorber in the visible range for these biomass burning aerosols.
45 Comparison with literature shows a consistent picture of increasing absorption enhancement of
46 biomass burning aerosol from emission to remote location and underscores that the evolution of
47 *SSA* occurred a long time after emission.
48 The results presented here build a fundamental basis of knowledge about the aerosol optical
49 properties observed over SWA during the monsoon season and can be used in climate modelling
50 studies and satellite retrievals. In particular and regarding the very high absorbing properties of
51 biomass burning aerosols over SWA, our findings suggest that considering the effect of internal
52 mixing on absorption properties of black carbon particles in climate models should help better
53 assessing the direct and semi-direct radiative effects of biomass burning particles.

54

55 **1. Introduction**

56 Atmospheric aerosols play a crucial role in the climate system by altering the radiation budget
57 through scattering and absorption of solar radiation and by modifying cloud properties and
58 lifetime. Yet considerable uncertainties remain about the contribution of both natural and
59 anthropogenic aerosol to the overall radiative effect (*Boucher et al., 2013*). Large uncertainties are
60 related to the complex and variable properties of aerosol particles that depend on the aerosol
61 source and nature as well as on spatial and temporal variations. During transport in the
62 atmosphere, aerosol particles may undergo physical and chemical aging processes altering the
63 composition and size distribution and henceforth the optical properties and radiative effects. The
64 capability of reproducing this variability in climate models represents a real challenge (*Myhre et*
65 *al., 2013; Stier et al., 2013; Mann et al., 2014*). Therefore, intensive experimental observations in
66 both aerosol source and remote areas are of paramount importance for constraining and evaluating
67 climate models.

68

69 Key parameters from a climate perspective are the aerosol vertical distribution and respective
70 spectral optical properties. Radiative transfer codes commonly incorporated in climate models and
71 in satellite data retrieval algorithms use single scattering albedo (*SSA*), extinction mass efficiency
72 (*MEE*) and asymmetry factor (*g*) as input parameters. These parameters depend on the aerosol size
73 distribution, the real and imaginary parts of the refractive index (*m-ik*), and the wavelength of
74 incident light, λ . The knowledge of the vertical distribution of these fundamental parameters is
75 crucial to accurately estimate the direct and semi-direct radiative effects of aerosols as well as the
76 vertical structure of atmospheric heating rates resulting from absorption by particles. Above
77 information is also required to retrieve aerosol properties (aerosol optical depth, size distribution)
78 from remote sensing data.

79

80 Southern West Africa (SWA) is one of the most climate-vulnerable region in the world , where the
81 surface temperature is expected to increase by $\sim 3^{\circ}\text{K}$ at the end of the century (2071-2100) in the
82 Coupled Model Intercomparison Project Phase 5 (CMIP5) (*Roehrig et al., 2013*). It is
83 characterized by a fast-growing population, industrialization and urbanization (*Lioussé et al.,*
84 *2014*). This is particularly the case along the Guinea Coast where several already large cities are
85 experiencing rapid growth (*Knippertz et al., 2015a*). Despite these dramatic changes, poor
86 regulation strategies of traffic, industrial and domestic emissions lead to a marked increase of
87 anthropogenic aerosol loading from multiple sources including road traffic, industrial activities,
88 waste burning, ship plumes, domestic fires, power plants, etc. Tangible evidence for regional
89 transport of anthropogenic pollutants associated with urban emissions has altered air pollution
90 from a local issue to a regional issue and beyond (*Deetz et al., 2018; Deroubaix et al. 2019*). This
91 is particularly the case during summer when land-sea breeze systems can develop and promote the
92 transport of pollutants inland, away from the urbanized coastal strip of SWA (*Flamant et al.,*
93 *2018a*). In addition to this anthropogenic regional pollution, SWA is impacted by a significant
94 import of aerosols from remote sources. Biomass burning mainly from vegetation fires in Central
95 Africa are advected to SWA in the marine boundary layer and aloft (*Mari et al., 2008; Menut et al.*
96 *2018; Haslett et al., 2019*). The nearby Sahara desert and the Sahel are large sources of natural
97 wind-blown mineral dust aerosol throughout the year with a peak in springtime (*Marticorena and*
98 *Bergametti, 1996*). Biomass burning, dust and anthropogenic pollution aerosols can be mixed
99 along their transport pathways (*Flamant et al., 2018a; Deroubaix et al. 2019*), resulting in
100 complex interactions between physical and chemical processes and even meteorological
101 feedbacks.

102

103 In West Africa, most of the aerosol–radiation interaction studies focused on optical properties of
104 dust and biomass burning aerosols in remote regions far from major sources of anthropogenic
105 pollution aerosol. They include ground-based and airborne field campaigns such as DABEX (Dust
106 and Biomass Experiment, *Haywood et al., 2008*), AMMA (Analysis Multidisciplinary of African
107 Monsoon, *Lebel et al., 2010*), DODO (Dust Outflow and Deposition to the Ocean, *McConnell et*
108 *al., 2008*), SAMUM-1 and SAMUM-2 (Saharan Mineral Dust Experiment, *Heintzenberg, 2009;*
109 *Ansmann et al., 2011*) and AER-D (AERosol Properties – Dust, *Ryder al. 2018*). These projects
110 concluded that the influence of both mineral dust and biomass burning aerosols on the radiation
111 budget is significant over West Africa, implying that meteorological forecast and regional/global
112 climate models should include their different radiative effects for accurate forecasts and climate
113 simulations. Over the Sahel region, *Solmon et al. (2008)* have highlighted the high sensitivity of
114 mineral dust optical properties to precipitation changes at a climatic scale. However, the optical
115 properties of aerosols particles in the complex chemical environment of SWA are barely studied.
116 This is partly due to the historically low level of industrial developments of the region. Motivated
117 by the quickly growing cities along the Guinea Coast, the study of transport, mixing, and feedback
118 processes of aerosol particles is therefore very important for better quantification of aerosol
119 radiative impact at the regional scale and improvement of climate and numerical weather
120 prediction models.

121

122 In this context, the DACCIWA (Dynamics-Aerosol-Chemistry-Clouds Interactions in West Africa,
123 *Knippertz et al., 2015b*) campaign, designed to characterize both natural and anthropogenic
124 emissions over SWA, provides important and unique observations of aerosols in a region much
125 more affected by anthropogenic emissions than previously thought. A comprehensive field
126 campaign took place in June–July 2016 including extensive ground-based (*Kalthoff et al., 2018*)
127 and airborne measurements (*Flamant et al., 2018b*). In this study, we present an overview of *in-*
128 *situ* airborne measurements of the vertical distribution of aerosol particles and their spectral optical
129 properties acquired with the ATR-42 French research aircraft over the Guinea Coast.

130

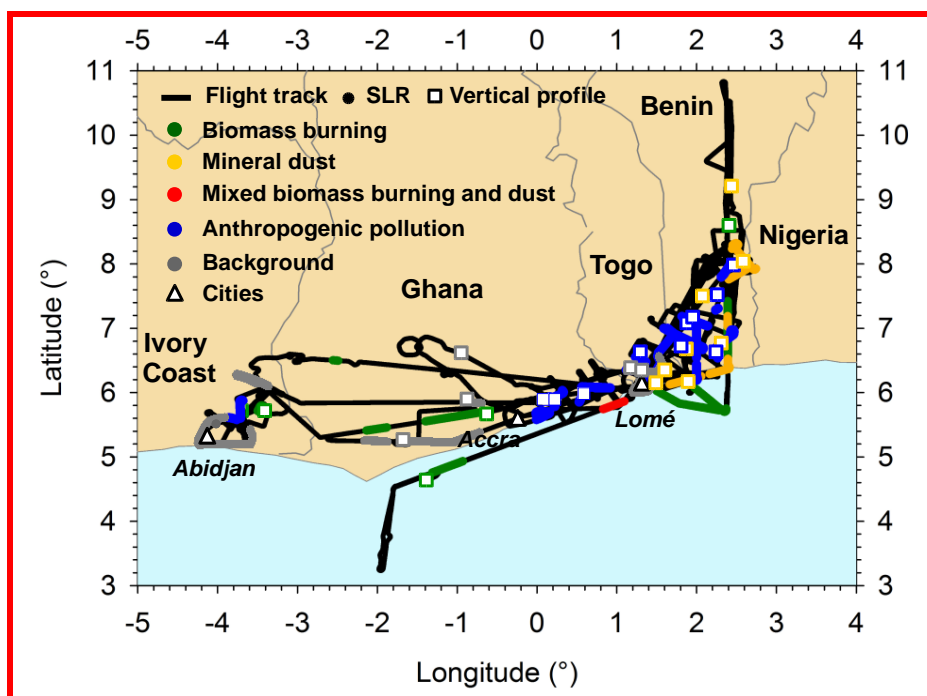
131 Section 2 presents the flight patterns, instrumentation and data analysis. Section 3 provides an
132 overview of the aerosol microphysical and optical properties. The impact of aging and mixing
133 processes on aerosol optical properties is discussed in section 4 before conclusions are presented in
134 section 5.

135

136 **2. Methodology**

137 **2.1. ATR-42 measurements overview**

138 This analysis focuses on flight missions conducted by the ATR-42 aircraft of SAFIRE (Service des
139 Avions Français Instrumentés pour la Recherche en Environnement - the French aircraft service
140 for environmental research) over the Gulf of Guinea and inland. A full description of flight
141 patterns during DACCIWA is given in *Flamant et al. (2018b)*. Here we present results from 15
142 flights focused on the characterization of anthropogenic pollution, dust and biomass burning
143 plumes. The flight tracks are shown in Figure 1 and a summary of flight information is provided in
144 Appendix 1. The sampling strategy generally consisted of two parts: first, vertical soundings were
145 performed from 60 m up to 8 km above mean sea level (amsl) to observe and identify interesting
146 aerosol layers. Subsequently, the identified aerosol layers were probed with the *in-situ* instruments
147 by straight levelled runs (SLR) at fixed flight altitudes.



148

149 **Figure 1. Tracks of the 15 flights analyzed in this study. The colors indicate aircraft flight**
150 **sampling layers dominated by biomass burning (green), mineral dust (orange), mixed dust-**
151 **biomass burning (red), anthropogenic pollution (blue) and background particles (grey) from**
152 **both vertical profiles (squares) and straight and level runs (SLRs; dots).**
153

154 The ATR-42 aircraft was equipped with a wide variety of instrumentation performing gas and
155 aerosol measurements. The measured meteorological parameters include temperature, dew point
156 temperature, pressure, turbulence, relative humidity, as well as wind speed and direction. Gas
157 phase species were sampled through a rear facing ¼ inch Teflon tube. Carbon monoxide (CO) was

158 measured using ultra-violet and infrared analysers (PICARRO). The nitric oxide (NO) and
159 nitrogen dioxide (NO₂) measurements were performed using an ozone chemiluminescence
160 instrument (Thermo Environmental Instrument TEi42C with a Blue Light Converter for the NO₂
161 conversion). On-board aerosol instruments sampled ambient air via stainless steel tubing through
162 the Community Aerosol Inlet (CAI). This is an isokinetic and isoaxial inlet with a 50 % sampling
163 efficiency for particles with a diameter of 5 μm (*Denjean et al., 2016*).

164

165 The total number concentration of particles larger than 10 nm (N_{tot}) was measured by a
166 condensation particle counter (CPC model MARIE built by University of Mainz; *Mertes,*
167 *Schröder, and Wiedensohler, 1995; Russell et al., 1996; Wiedensohler et al., 1997*). The aerosol
168 size distribution was measured using an ultra-high sensitivity aerosol spectrometer (UHSAS,
169 DMT), a custom-built scanning mobility sizer spectrometer (SMPS) and an optical particle counter
170 (OPC, GRIMM model 1.109). Instrument calibration was performed with PSL nanospheres and oil
171 particles size-selected by a differential mobility analyser (DMA) for diameters from 90 nm to 20
172 μm. The SMPS data acquisition system failed after two-third of the campaign and could not be
173 repaired. We found the UHSAS to show false counts in the diameters below 100 nm. Therefore,
174 these channels were disregarded in the data analysis.

175

176 The particle extinction coefficient (σ_{ext}) at the wavelength of 530 nm was measured with a cavity
177 attenuated phase shift particle light extinction monitor (CAPS-PMex, Aerodyne Research). The
178 particle scattering coefficients (σ_{scat}) at 450, 550 and 635 nm were measured using a TSI 3-
179 wavelength nephelometer and corrected for angular truncator error in the data inversion procedure
180 using a Mie code (i.e. Section 2.3.1 and Appendix 2). The absorption coefficients (σ_{abs}) at 467, 520
181 and 660 nm were measured by a Radiance Research Particle Soot Absorption Photometer (PSAP).
182 The PSAP measures changes of filter attenuation due to the collection of aerosol deposited on the
183 filter, which were corrected for the scattering artifacts according to the *Virkkula (2010)* method.
184 Prior to the campaign, the CAPS was evaluated against the combination of the nephelometer and
185 the PSAP. An instrument intercomparison was performed with purely scattering ammonium sulfate
186 particles and with strongly absorbing black carbon particles (BC). Both types of aerosol were
187 generated by nebulizing a solution of the respective substances and size-selected using a DMA.
188 For instrument intercomparison purposes, σ_{ext} from the combination of nephelometer and PSAP
189 was adjusted to that for 530 nm by using the scattering and absorption Ångström exponent (*SAE*
190 and *AAE*, respectively). The instrument evaluation showed an excellent accuracy of the CAPS
191 measurements by comparison to the nephelometer and PSAP combination.

192 **2.2. Ancillary products**

193 In order to determine the history of air masses prior aircraft sampling, backward trajectories and
194 satellite images were used. The trajectories were computed using the Hybrid Single Particle
195 Lagrangian Integrated Trajectory Model (HYSPLIT) and the National Centers for Environmental
196 Prediction (NCEP) Global Data Assimilation System (GDAS) data with 0.5° horizontal resolution
197 for sequences and times of interest. We compared the backward trajectory heights with information
198 of fire burning times (e.g. MODIS Burnt Area Product) and dust release periods (e.g. Meteosat
199 Second Generation (MSG) dust RGB composite images) to assess the aerosol source regions of the
200 investigated air masses. The air masses represented by the trajectory are assumed to obtain their
201 aerosol loading from source regions when the trajectory passes over regions with significant dust
202 activation and/or fire activity at an altitude close to the surface. Trajectory calculations with
203 slightly modified initial conditions with respect to the arrival time, location and altitude were
204 performed to check the reliability of the location of source regions. Uncertainties in this approach,
205 caused by unresolved vertical mixing processes, and by general uncertainties of the trajectory
206 calculations are estimated to be in the range of 15–20 % of the trajectory distance (*Stohl et al.*,
207 2002).

208

209 **2.3. Data analysis**

210 In the following, extensive aerosol parameters (concentrations, scattering, absorption and
211 extinction coefficients) are converted to standard temperature and pressure (STP) using $T = 273$ K
212 and $P = 1013.25$ hPa. The STP concentration data correspond to mixing ratios, which are
213 independent of ambient pressure and temperature during the measurement. In the analysis, the data
214 were averaged over sections of SLR with homogeneous aerosol conditions outside of clouds.

215

216 **2.3.1. Derivation of aerosol microphysical and optical properties**

217 Appendix 2 and Table 1 show the iterative procedure and the equations used to calculate the
218 aerosol microphysical and optical parameters as briefly explained below.

219

220 The particle number concentration in the coarse mode (N_{coarse}) was calculated by integrating the
221 OPC size distributions over the range 1 to 5 μm . **The signal to noise ratio of the OPC for particles
222 in this size range was higher than 3, which makes the instrument well suited to quantify variations
223 in N_{coarse} .** The number concentration of particles in the fine mode (N_{fine}) was obtained as the
224 difference between total number concentration (N_{tot} particle diameter range above 5 nm) measured
225 by the CPC and N_{coarse} .

226

227 For optical calculations, the $3\lambda\text{-}\sigma_{abs}$ from the PSAP were adjusted at the 3 wavelengths measured
228 by the nephelometer using the *AAE* calculated from the 3λ measured σ_{abs} . Once σ_{scat} and σ_{abs}
229 obtained at the same wavelength, an optical closure study estimated the complex refractive index
230 based on optical and size data. Optical calculations were performed using Mie theory, **implying a**
231 **sphericity assumption, because it facilitates a quantitative comparison with past data, mostly using**
232 **this simplification and because most climate models assume spherical properties. The retrieval**
233 **algorithm consists of iteratively varying** the real part of the complex refractive index (m) from 1.33
234 to 1.60 and the imaginary part of the complex refractive index (k) from 0.000 to 0.080 in steps of
235 resolution of 0.001. **m and k were fixed when the difference between calculated values of σ_{scat} and**
236 **σ_{abs} and measurements was below 1%.** Given that the size distribution measured by the UHSAS
237 and the OPC depends on n , the optical-to-geometrical diameter conversion was recalculated at
238 each iteration based on the assumed n . The resulting number size distributions from SMPS,
239 UHSAS and OPC were parameterized by fitting four log-normal distributions and used as input
240 values in the optical calculations. Once n and k were obtained at 3λ , we estimated the following
241 optical parameters:

242 - *SAE* depends on the size of the particles. Generally, it is lower than 0 for aerosols dominated by
243 coarse particles, such as dust aerosols, but it is higher than 0 for fine particles, such as
244 anthropogenic pollution or biomass burning aerosol (*Seinfeld and Pandis, 2006; Schuster et al.,*
245 *2006*).

246 - *AAE* provides information about the chemical composition of atmospheric aerosols. BC absorbs
247 radiation across the whole solar spectrum with the same efficiency, thus it is characterized by *AAE*
248 values around 1. Conversely, mineral dust particles show strong light absorption in the blue to
249 ultraviolet spectrum leading to *AAE* values up to 3 (*Kirchstetter et al., 2004; Petzold et al., 2009*).

250 - *SSA* describes the relative importance of scattering and absorption for radiation. Thus, it indicates
251 the potential of aerosols for cooling or warming the lower troposphere.

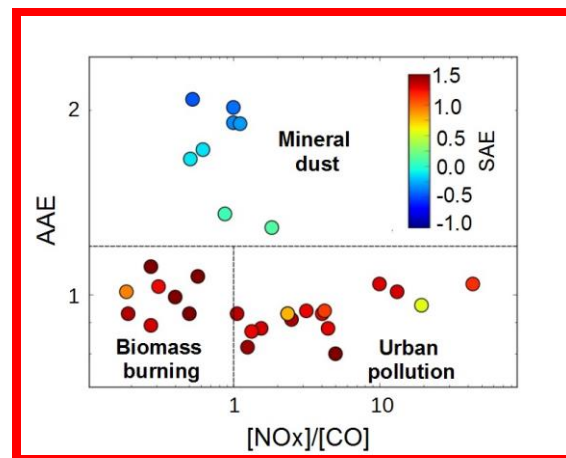
252 - g describes the probability of radiation to be scattered in a given direction. Values of g can range
253 from -1 for entirely backscattered light to $+1$ for complete forward scattering light.

254 - ***MEE*** represents the total light extinction per unit mass concentration of aerosol. The estimates of
255 ***MEE*** assume mass densities of 2.65 g cm^3 for dust aerosol, 1.35 g cm^3 for biomass burning
256 aerosol, 1.7 g cm^3 for anthropogenic aerosol and 1.49 g cm^3 for background aerosol (*Hess et al.,*
257 *1998; Haywood et al., 2003a*).

Aerosol parameters	Symbol	λ (nm)	Method
Aerosol microphysical properties			
Total number concentration	N_{tot}	-	Measured by a CPC in the particle diameter range above 5 nm
Number concentration in the coarse mode	N_{coarse}	-	GRIMM size distributions integrated on the range 1 to 5 μm .
Number concentration in the fine mode	N_{fine}	-	Difference N_{tot} and N_{coarse} .
Number size distribution	$dN/d\log D_p$	-	$dN/d\log D_p = \sum_{i=1}^4 (N_{tot,i} \exp(-(\log D_p - \log D_{p,g,i})^2 / (2 \log \sigma_i)) / (\sqrt{2 \log \sigma_i}))$ with $N_{tot,i}$ the integrated number concentration, $D_{p,g,i}$ the geometric median diameter and σ_i geometric standard deviation for each mode i
Volume size distribution	$dV/d\log D_p$	-	$dV/d\log D_p = \sum_{i=1}^4 (N_{tot,i} D_p^3 \pi / 6 \exp(-(\log D_p - \log D_{p,g,i})^2 / (2 \log \sigma_i)) / (\sqrt{2 \log \sigma_i}))$
Aerosol optical properties			
Scattering coefficient	σ_{scat}	450, 550, 635	Measured by the nephelometer and corrected for truncator error
Absorption coefficient	σ_{abs}	467, 520, 660	Measured by the PSAP and corrected for filter based artefacts
Extinction coefficient	σ_{ext}	530	Measured by the CAPS
Scattering Ångström exponent	SAE	450 to 700	Calculated from the nephelometer measurements : $SAE = -\ln(\sigma_{scat}(450)/\sigma_{scat}(700)) / \ln(450/700)$
Absorption Ångström exponent	AAE	440 to 660	Calculated from the PSAP measurements : $AAE = -\ln(\sigma_{abs}(467)/\sigma_{abs}(660)) / \ln(467/660)$
Complex refractive index	n	450, 550, 660	Inversion closure study using Mie theory (Fig. A2) $n(\lambda) = m(\lambda) - ik(\lambda)$
Single scattering albedo	SSA	450, 550, 660	Inversion closure study using Mie theory (Fig. A2) $SSA(\lambda) = \sigma_{scat}(\lambda) / \sigma_{ext}(\lambda)$
Mass extinction efficiency	MEE	450, 550, 660	Inversion closure study using Mie theory (Fig. A2) $MEE(\lambda) = \sigma_{ext}(\lambda) / C_m$ with C_m the aerosol mass concentration
Asymmetry parameter	g	450, 550, 660	Inversion closure study using Mie theory (Fig. A2) $g(\lambda) = 1/2 \int_0^\pi \cos(\Theta) \sin(\Theta) P(\Theta, \lambda) d(\Theta)$ with $P(\Theta, \lambda)$ the scattering phase function and Θ the scattering angle.

261 2.3.2. Classification of aerosols plumes

262 Data were screened in order to isolate plumes dominated by anthropogenic pollution from urban
263 emissions, biomass burning and mineral dust particles, resulting in a total number of 19, 12 and 8
264 genuine plume interceptions, respectively, across the 15 flights. As shown in Figure 2,
265 identification of the plumes was based on a combination of CO and NO_x (sum of NO and NO₂)
266 concentrations, as well as AAE and SAE that have been shown to be good parameters for
267 classifying aerosol types (Kirchstetter et al., 2004; Petzold et al., 2009). The classification was
268 then compared with results from the back trajectory analysis (Figure 3) and satellite images
269 described in section 2.2.



270

271 **Figure 2. Absorption Ångström Exponent (AAE) as a function of the ratio NO_x to CO. The**
272 **markers are colored according to the Scattering Ångström Exponent (SAE). Classification of**
273 **mineral dust, biomass burning and urban pollution particles has been added to the figure.**
274

275 The guidelines for classification are as follows:

276 - *Anthropogenic pollution*: SAE was beyond threshold 0, indicating a large number fraction of
277 small particles in urban plumes, and CO and NO_x concentrations 2 times higher than the
278 background concentrations. During the DACCIWA campaign background CO and NO_x values
279 were around 180 ppb and 0.28 ppb, respectively. The trajectories show large differences in the
280 flow patterns and source regions with urban plumes originating from the polluted cities of Lomé,
281 Accra and Abidjan. The aircraft sampling over land mostly followed the north-eastward direction
282 (Figure 3d).

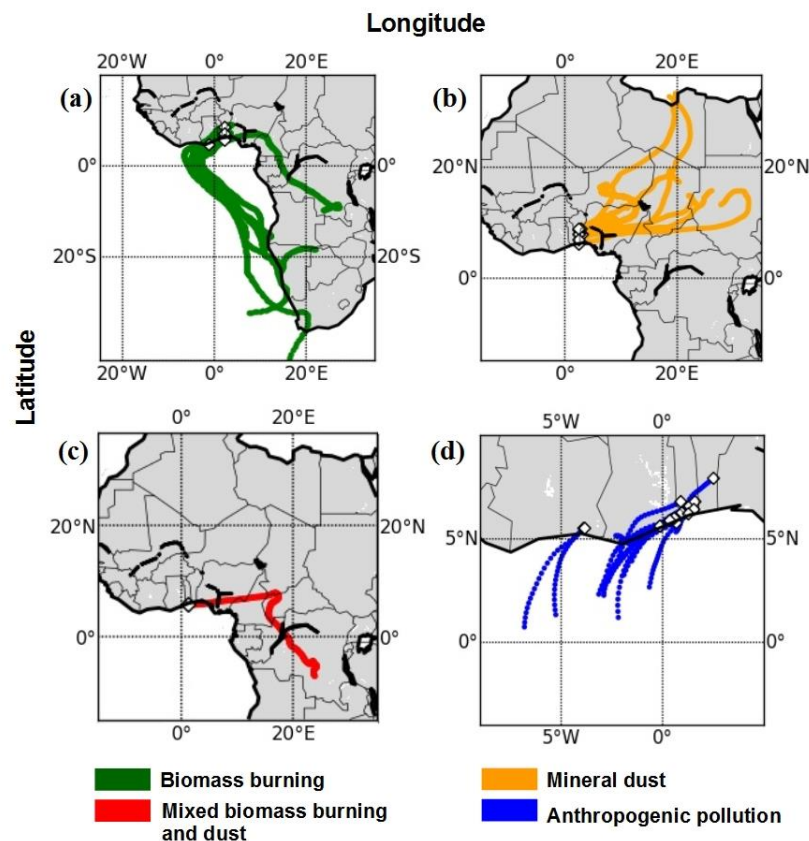
283 - *Biomass burning*: The criteria are the same as for urban pollution plumes except that trajectories
284 track these plumes back to active fire hotspots as observed by MODIS and the ratio NO_x to CO
285 was set below 1. CO and NO_x are byproducts of combustion sources but CO is preserved longer
286 along the plume when compared with NO_x, which makes the ratio NO_x to CO a good indicator for
287 distinguishing fresh anthropogenic pollution plumes from biomass burning plumes transported

288 over long distances (Wang et al., 2002; Silva et al., 2017). During this time of the year, most of the
289 forest and grassland fires were located in Central and Southern Africa (Figure 3a).

290 - *Mineral dust*: AAE higher than 1 indicates a large mass fraction of mineral dust and a SAE below
291 0 indicate a high effective particle diameter. The source region of the dust loaded air masses was
292 located in the Saharan desert and in the Sahel (Figure 3b).

293 - *Dust and biomass burning mixing*: Combining remote sensing observations and model
294 simulations, Flamant et al. (2018a) identified a biomass burning plume mixed with mineral dust.
295 This agrees well with the measured AAE of 1.2 and SAE of 0.3 observed in this layer. Menut et al.
296 (2018) have shown that one of the transport pathways of biomass burning aerosols from Central
297 Africa was associated with northward advection towards Chad and then westward displacement
298 linked to the African Easterly Jet. The plume originated from a broad active biomass burning area
299 including Gabon, the Republic of Congo and the Democratic Republic of Congo and passed over
300 areas with strong dust emissions further north within 1–3 days before being sampled by the aircraft
301 (Figure 3c).

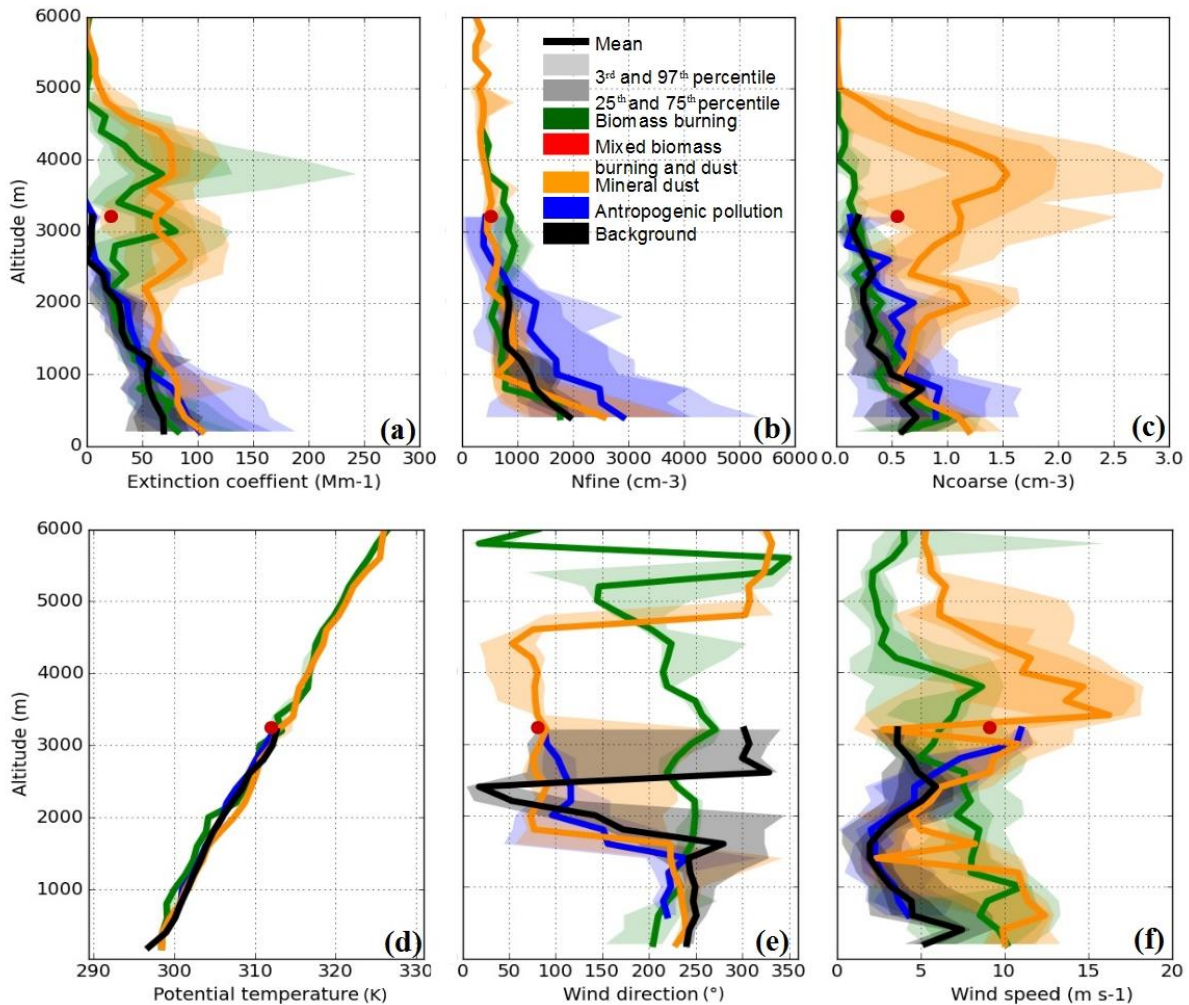
302 - *Background*: We refer to background conditions as an atmospheric state in the boundary layer
303 without the detectable influence of mineral dust, biomass burning or local anthropogenic sources.
304 Most back trajectories originated from the marine atmosphere and coastal areas south of the
305 sampling area.



306 **Figure 3. Backward trajectories for the analyzed aerosol layers. Trajectories date back 10**
 307 **days for (a), 5 days for (b) and (c), and 1 day for (d).**
 308

309 **3.1. Aerosol vertical distribution**

310 Figure 4 shows a statistical analysis of N_{fine} , N_{coarse} and σ_{ext} derived from the *in-situ* measurements
 311 of vertical profiles. The aerosol vertical structure is strongly related to the meteorological structure
 312 of the atmosphere (see Knippertz *et al.*, 2017 for an overview of the DACCIWA field campaign).
 313 Therefore wind vector and potential temperature profiles acquired with the aircraft have been
 314 added to Figure 4 as a function of the dominating aerosol composition, introduced in Figure 1. The
 315 data from individual vertical profiles were merged into 200 m vertical bins from the surface to 6
 316 km amsl. The profiles were calculated using only individual profiles obtained outside of clouds.
 317



318 **Figure 4. Vertical layering of aerosols and meteorological variables for profiles for which**
 319 **aerosols dominated by biomass burning (green), dust (orange), mixed dust-biomass burning**
 320 **(red), anthropogenic pollution (blue) and background particles (black) were detected. The**
 321 **panels show profiles of (a) the extinction coefficient at 530 nm, (b) the particle number**

322 concentration in the range $0.005 < D_p < 1 \mu\text{m}$, (c) the particle number concentration in the
323 range $1 < D_p < 5 \mu\text{m}$, (d) potential temperature, (e) the wind direction and (f) the wind speed.
324 The colored areas represent the 3th, 25th, 75th and 97th percentiles of the data. The mixed dust-
325 biomass burning plume is represented by a dot because it is derived from measurements
326 during a SLR.

327

328 The observed wind profiles highlight the presence of several distinct layers in the lower
329 troposphere. For cases related to dust, urban pollution and background condition, we clearly
330 observe the monsoon layer up to 1.5 km amsl which is characterized by weak to moderate wind
331 speeds (2 to 10 m s⁻¹, the later corresponding to dust cases) and a flow from the southwest (220-
332 250°). In all three air mass regimes, the monsoon layer is topped by a 500 to 700 m deep layer
333 characterised by a sharp wind direction change (from south-westerly to easterly). Weak wind
334 speeds (less than 5 m s⁻¹) are observed in urban pollution and background conditions, while higher
335 wind speeds are observed in the dust cases. Above 2.5 km amsl, the wind speed increases in the
336 urban pollution and dust cases and the wind remains easterly, indicating the presence of the
337 African easterly jet with its core typically farther north over the Sahel (Figure 8 in Knippertz *et al.*,
338 2017 for the latitudinal variations of the African easterly jet during the DACCWA field phase).
339 The maximum easterlies are observed in the dust cases slightly below 3.5 km amsl (> 15 m s⁻¹).
340 For the background cases, the wind above the shear layer shifts to north-westerly and remains
341 weak (~i.e. 5 m s⁻¹). Overall, the wind profile associated with the biomass burning cases is quite
342 different from the other three cases, with a flow essentially from the south-southwest below 5 km
343 amsl and higher wind speeds in the lower 2 km amsl than above, and a secondary maximum of 7
344 m s⁻¹ at 4 km amsl.

345

346 The vertical distribution of aerosol particles was very inhomogeneous, both across separate
347 research flights and between individual plumes encountered during different periods of the same
348 flight. Measurements of aerosols within this analysis cover a broad geographic region, as shown in
349 Figure 1, which may explain some of the variability. SWA is subject to numerous anthropogenic
350 emission sources (e.g. road traffic, heavy industries, open agriculture fires, etc.) coupled to
351 biogenic emissions from the ocean and forests. These resulting large emissions are reflected in the
352 high variability of σ_{ext} , N_{fine} and N_{coarse} in the lower troposphere over SWA. Below 2.5 km amsl, σ_{ext}
353 showed a large heterogeneity with values ranging from 35 to 188 Mm⁻¹ between the 3rd and 97th
354 percentile and a median value of 55 Mm⁻¹. The variability of σ_{ext} values was slightly enhanced near
355 the surface and was correlated to N_{fine} and N_{coarse} which ranged from 443 to 5250 cm⁻³ and from
356 0.15 to 1.6 cm⁻³, respectively. Maximum surface σ_{ext} was recorded in the anthropogenic pollution
357 plume of Accra where high N_{fine} was sampled. The aerosol vertical profile is strongly modified

358 during biomass burning and dust events. The dust plume extends from 2 to 5 km amsl, and is
359 associated with transport from the dust sources in Chad and Sudan (see Figure 3) with the midlevel
360 easterly flow. The biomass burning plume extends from 1.5 to 5 km amsl and is associated with
361 transport from the southwest in a layer of enhanced wind speed just below 4 km amsl as discussed
362 above. Both layers showed enhanced σ_{ext} with median values of 68 Mm^{-1} ($p_{03} = 12 \text{ Mm}^{-1}$; $p_{97} = 243$
363 Mm^{-1}) in biomass burning plumes and 78 Mm^{-1} ($p_{03} = 45 \text{ Mm}^{-1}$; $p_{97} = 109 \text{ Mm}^{-1}$) in dust plumes.
364 As expected, the extinction profile was strongly correlated to N_{fine} for biomass burning layers and
365 N_{coarse} for dust layers.

366

367 A prominent feature in the vertical profiles is the presence of fine particles up to 2.5 km amsl
368 outside of biomass burning or dust events. σ_{ext} , N_{fine} and N_{coarse} continuously decrease with altitude,
369 most likely due to vertical mixing of local emissions from the surface to higher levels. Therefore,
370 the regional transport of locally emitted aerosols was not limited to the surface but occurred also at
371 higher altitude. Recently, numerical tracer experiments performed for the DACCIWA airborne
372 campaign period have demonstrated that a combination of land–sea surface temperature gradients,
373 orography-forced circulation and the diurnal cycle of the wind along the coastline favor the
374 vertical dispersion of pollutants above the boundary layer during daytime (*Deroubaix et al., 2019*;
375 *Flamant et al., 2018a*). Because of these complex atmospheric dynamics, aerosol layers transiting
376 over the Gulf of Guinea in the free troposphere could be contaminated by background or urban
377 pollution aerosols from the major coastal cities.

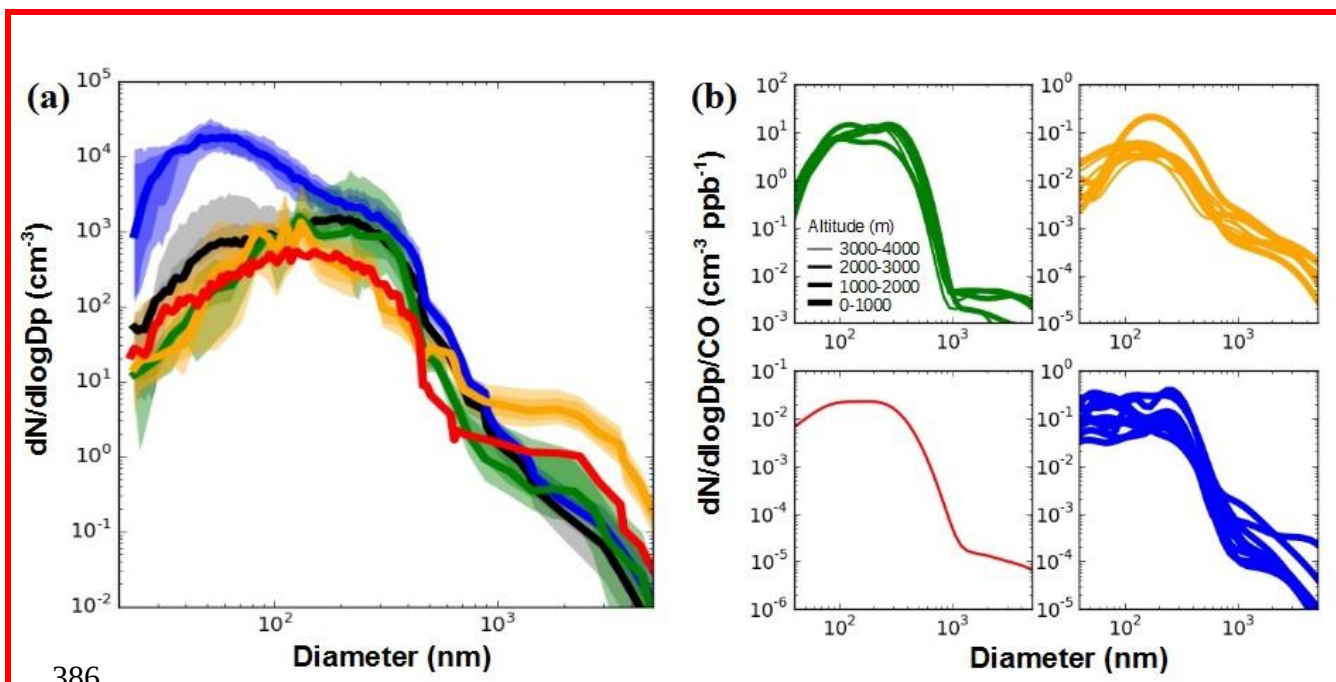
378

379 **3.2. Aerosol size distribution**

380 Figure 5a shows the range of variability of the number and volume size distributions measured
381 during DACCIWA. These are extracted from the SLRs identified in Fig.1. Figure 5b shows the
382 same composite distribution normalized by CO concentration in order to account for differences in
383 the amount of emissions from combustion sources.

384

385



386
 387 **Figure 5. (a) Statistical analysis of number size distributions with colored areas representing**
 388 **the 3th, 25th, 75th and 97th percentiles of the data and (b) number size distributions normalized**
 389 **to CO for plumes dominated by biomass burning (green), dust (orange), mixed dust-biomass**
 390 **burning (red), anthropogenic pollution (blue) and background particles (black). In panel b,**
 391 **the line thickness is scaled by the altitude of the aerosol plume.**
 392

393 Considerable variability in the number concentration of the size distributions, up to approximately
 394 2 orders of magnitude, was observed for a large fraction of the measured size range. The size
 395 distributions varied both for different aerosol types and for a given aerosol class. This reflects the
 396 relative wide range of different conditions that were observed over the region, both in terms of
 397 sources, aerosol loading, and lifetimes of the plumes.

398

399 In particular for ultrafine particles with diameters below 100 nm, large differences are observed,
 400 with an increase as large as a factor of 50 in urban plumes, which reflects concentration increase
 401 from freshly formed particles. Interestingly elevated number concentrations of these small-
 402 diameter particles were also observed in some dust layers. Comparing the particle size distribution
 403 of the different dust plumes sampled during the field campaign, a variation as large as a factor of
 404 20 in the number concentration of ultrafine particles is found (i.e. Figure 4). Their contribution
 405 decreased with height as reflected by higher small particle number recorded in dust plumes below
 406 2.5 km amsl (Figure 4b and 5b). As the composite urban size distributions showed a relatively
 407 similar ultrafine mode centered at 50 nm, dust layers have most likely significant contributions
 408 from anthropogenic pollution aerosol freshly emitted in SWA. The ultrafine mode was not

409 observed in biomass burning size distributions, even though dust and biomass burning plumes
410 were sampled in the same altitude range. We interpret this observation with dust plumes
411 transported below 2.5 km amsl that were sampled over the region of Savè (8°01'N, 2°29'E; Benin)
412 near the identified urban air mass transported northeastwards from Lomé and/or Accra and which
413 may have collected significant fresh pollution on their way, whereas biomass burning plumes
414 collected at the same altitude and sampled over Ivory Coast south of the Abidjan pollution plumes
415 may not have been affected by significant direct pollution (Figure 1).

416

417 The accumulation mode was dominated by two modes centered at $D_{p,g} \sim 100$ and 230 nm
418 depending on the aerosol plume. The particle size distributions for biomass burning plumes were
419 generally dominated by an accumulation mode centered at $D_{p,g} \sim 230$ nm. Despite the relative wide
420 range of sources and lifetimes of the biomass burning plumes sampled throughout the campaign
421 (Figure 3), the $D_{p,g}$ in the accumulation mode showed little variation ($D_{p,g}$ from 210 to 270 nm)
422 between the plumes. Similarly, previous field studies found accumulation mode mean diameters
423 from 175 to 300 nm for aged biomass burning plumes, regardless of their age, transport time and
424 source location (Capes *et al.*, 2008; Janhäll *et al.*, 2010; Weinzierl *et al.*, 2011; Sakamoto *et al.*,
425 2015; Carrico *et al.* 2016). The coagulation rate can be very high in biomass burning plumes and
426 can shape the size distribution over a few hours (Sakamoto *et al.*, 2016). It is worth noting that in
427 the biomass burning and dust size distributions there is a persistent particle accumulation mode
428 centered at ~ 100 nm that exceeds the amount of **particles centered at 230 nm** in some layers. This
429 small mode is unlikely to be related to long-range transport of biomass burning and Saharan dust
430 emissions, as it would be expected that particles in this size range would grow to larger particles
431 through coagulation relatively quickly. As similar concentrated accumulation modes of particles
432 have been observed in background plumes, it suggests the entrainment of background air from the
433 boundary layer in dust and biomass burning plumes. ~~This is supported by remote sensing
434 observations on 2 and 5 July 2016 (Flamant *et al.*, 2018a; Deroubaix *et al.*, 2019).~~

435

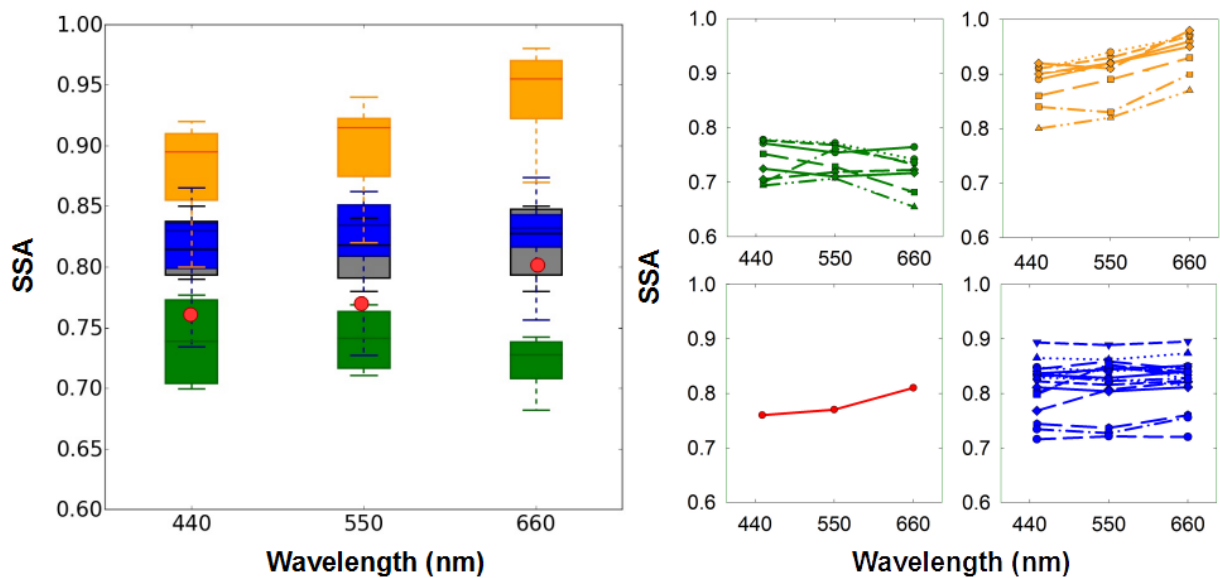
436 The number concentration of large super-micron particles was strongly enhanced in the mineral
437 dust layers. The peak number concentration displayed a broad shape at $D_{p,g} \sim 1.8 \mu\text{m}$, which is
438 comparable to literature values of other long-range transported dust aerosols (Weinzierl *et al.*,
439 2011; Ryder *et al.*, 2013; Denjean *et al.*, 2016; Liu *et al.*, 2018). **The super-micron mode of the
440 dust plume is expected to be impacted by the mixing with other particles in case of an internal
441 mixing, which should somewhat increase the particle size.** The relatively homogeneous $D_{p,g}$ in the
442 coarse mode of dust reported here ($D_{p,g}$ from 1.7 to 2.0 μm) suggests low internal mixing with

443 other atmospheric species. Besides, the volume size distribution in urban plumes showed
 444 significant presence (~ 65% of the total aerosol volume) of large particles with diameters of ~ 1.5
 445 – 2 μm , which were also observed in background conditions. We measured AAE in the range 0.7-
 446 1 in anthropogenic pollution plumes (Figure 2), which suggests negligible contribution of mineral
 447 dust in these plumes. This coarse mode has most likely significant contributions from sea salt
 448 particles, as plumes arriving from the cities were transported at low altitude over the ocean (Fig.
 449 3).

450

451 3.3. Aerosol optical properties

452 SSA is one of the most relevant intensive optical properties because it describes the relative
 453 strength of the aerosol scattering and absorption capacity and is a key input parameter in climate
 454 models (Solmon *et al.*, 2008). Figure 6 shows the spectral SSA for the different SLRs considered in
 455 this study.



456

457 **Figure 6. (a) Statistical analysis of single scattering albedo at 450, 550 and 660 nm for**
 458 **plumes dominated by biomass burning (green), dust (orange), mixed dust-biomass burning**
 459 **(red), anthropogenic pollution (blue) and background particles (black). The boxes enclose the**
 460 **25th and 75th percentiles, the whiskers represent the 5th and 95th percentiles and the**
 461 **horizontal bar represents the median. (b) Spectral SSA for the different individual plumes**
 462 **considered in this study. The mixed dust-biomass burning plume is represented by a dot**
 463 **because it is derived from measurements during only one SLR.**
 464

465 The highest absorption (lowest SSA) at all three wavelengths was observed for biomass burning
 466 aerosols. SSA values ranged from 0.69–0.78 at 440 nm, 0.71–0.77 at 550 nm and 0.65–0.76 at 660

467 nm. This is on the low side of the range of values (0.73–0.93 at 550 nm) reported over West Africa
468 during DABEX for biomass burning plumes mixed with variable proportion of mineral dust
469 (*Johnson et al., 2008*). No clear tendency was found for the spectral dependence of SSA, which in
470 some of the cases decreased with wavelength and in others were very similar to each other at all
471 three wavelengths. ~~The strongest spectral dependence of SSA was observed for biomass burning~~
472 ~~plumes with the lowest absorption (highest SSA) at 440 nm. Laboratory experiments have shown~~
473 ~~that strongly absorbing biomass burning particles tend to have a weak wavelength dependent~~
474 ~~absorption, while weakly light absorbing particles tend to have a strong wavelength dependent~~
475 ~~absorption (*McMeeking et al., 2014; Zhai et al., 2017*), which is consistent with results in this~~
476 ~~study.~~

477

478 SSA values of anthropogenic pollution aerosols were generally intermediate in magnitude with
479 median values of 0.81 at 440 nm, 0.82 at 550 nm and 0.82 at 660 nm. Our data show that the value
480 of SSA varied significantly for the different plumes. Some pollution aerosols absorb almost as
481 strongly as biomass burning aerosols with SSA(550nm) values as low as 0.72, whereas the highest
482 SSA(550nm) value observed was 0.86. In addition, the absorption properties of urban aerosol
483 varied greatly between the sampled plumes for smoke of apparent same geographic origin. For
484 example, we measured SSA(550nm) values from 0.72 to 0.82 in the Accra pollution outflow. The
485 variability in SSA values may be due to the possible contribution of emissions from different cities
486 to the sampled pollution plumes (*Deroubaix et al., 2019*), thus having different combustion
487 sources and chemical ages. Past in-situ measurements of aerosol optical properties over SWA cities
488 appear, unfortunately, to be absent from literature. However, the flat spectral dependence of SSA
489 appears to be anomalous for anthropogenic pollution aerosols, as SSA ~~is~~ has been shown to
490 ~~xpected~~ decrease with increasing wavelength for a range of different urban pollution plumes over
491 ~~European, American and Asian cities (*Dubovick et al., 2002; Di Biagio et al., 2016; Shin et al.,*~~
492 ~~2019). As during DACCIWA SSAs of anthropogenic pollution aerosols reached similar values to~~
493 ~~those of background aerosols, it suggests a large contribution of the latter to the aerosol optical~~
494 ~~properties of the mixture.~~

495

496 The magnitude of SSA increased at the three wavelengths when dust events occurred. ~~It is~~
497 ~~important to note that the measurements exclude a significant portion of the coarse mode aerosol~~
498 ~~due to poor inlet passing efficiency of larger aerosol particles (a 50% size cut around 5 μ m), which~~
499 ~~may result in an overestimate of SSA. Despite this limitation, our measurements are comparable to~~
500 ~~one another and to previous in-situ measurements by taking into account the sampling inlet.~~ Large

501 variations in *SSA* were obtained with values ranging from 0.76–0.92 at 440 nm, 0.81–0.94 at 550
502 nm and 0.81–0.97 at 660 nm. The measurement of *SSA* is highly dependent on the extent to which
503 the coarse mode is measured behind the aerosol sampling inlet. *Denjean et al. (2016)* found that
504 the absolute error associated with *SSA*, *g* and *MEE* of dust aerosols due to the CAI inlet is in the
505 range covered by the measurement uncertainties. However, different aerosol inlet systems were
506 used during previous field campaigns, which makes comparison of our results with previous
507 measurements difficult. Overall, compared with the literature for transported dust, lower values
508 were obtained in the present study for few cases. For example, *Chen et al. (2011)* reported
509 *SSA*(550 nm) values of 0.97 ± 0.02 during NAMMA (a part of AMMA operated by NASA) using
510 an inlet with a comparable sampling efficiency. The lower values from DACCIWA reflect
511 inherently more absorbing aerosols in some dust plumes. In contrast to fire plumes, the *SSA* of
512 dust aerosol showed a clear increasing trend with wavelength. This behavior is likely due to the
513 domination of large particles in dust aerosol, which is in agreement to similar patterns observed in
514 dust source regions (*Dubovik et al., 2002*). Moreover, an increase of *SSA* is observed with
515 wavelength for mixed dust-smoke aerosol, suggesting that the aerosol particles were
516 predominantly from dust, albeit mixed with a significant loading of biomass burning.

		<i>SSA(450)</i>	<i>SSA(550)</i>	<i>SSA(660)</i>	<i>MEE(450)</i>	<i>MEE(550)</i>	<i>MEE(660)</i>	<i>g(450)</i>	<i>g(550)</i>	<i>g(660)</i>	<i>SAE</i>
Mineral dust	median	0.88	0.90	0.93	0.74	0.68	0.66	0.74	0.72	0.69	-0.35
	3 th	0.82	0.82	0.86	0.38	0.38	0.39	0.69	0.67	0.65	-0.56
	25 th	0.85	0.87	0.90	0.43	0.43	0.43	0.73	0.72	0.67	-0.48
	75 th	0.91	0.93	0.96	0.94	0.85	0.85	0.75	0.74	0.72	-0.25
	97 th	0.92	0.95	0.97	1.57	1.37	1.21	0.78	0.76	0.72	-0.12
Biomass burning	median	0.74	0.76	0.72	1.91	1.62	1.34	0.69	0.68	0.61	1.07
	3 th	0.70	0.72	0.66	0.94	1.45	1.22	0.64	0.65	0.59	0.59
	25 th	0.70	0.76	0.71	1.67	1.48	1.27	0.69	0.65	0.60	0.83
	75 th	0.77	0.77	0.74	1.86	1.65	1.55	0.72	0.68	0.62	1.15
	97 th	0.78	0.77	0.76	2.38	1.92	1.58	0.73	0.68	0.63	1.64
Mixed dust-Biomass burning	median	0.76	0.77	0.81	1.58	1.40	1.30	0.73	0.66	0.64	0.38
	3 th	-	-	-	-	-	-	-	-	-	-
	25 th	-	-	-	-	-	-	-	-	-	-
	75 th	-	-	-	-	-	-	-	-	-	-
	97 th	-	-	-	-	-	-	-	-	-	-
Anthropogenic Pollution	median	0.83	0.84	0.85	2.60	2.49	1.90	0.60	0.61	0.62	0.75
	3 th	0.78	0.79	0.81	0.70	1.24	0.54	0.60	0.59	0.54	0.30
	25 th	0.80	0.82	0.83	2.14	2.25	1.53	0.62	0.60	0.56	0.65
	75 th	0.84	0.86	0.85	3.51	2.96	2.53	0.69	0.62	0.67	0.89
	97 th	0.87	0.88	0.90	3.70	4.83	2.74	0.73	0.64	0.70	0.94

518

519 **Table 2. Single scattering albedo, extinction mass efficiency, asymmetry parameter, single**
520 **scattering albedo and scattering Ångström exponent for the dominant aerosol classification.**

521

522 As shown in Table 2, the observed variability of SSA reflects a large variability for *MEE* at 550nm,
523 which spans a wide range from 0.38 to 1.37 m² g⁻¹, 1.45 to 1.92 m² g⁻¹ and 1.24 to 4.83 m² g⁻¹ for
524 dust, biomass burning for anthropogenic polluted aerosols, respectively. *MEE is heavily*
525 *influenced by the mass concentrations in the accumulation mode where the aerosol is optically*
526 *more efficient in extinguishing radiation. We found MEE to be positively correlated with SAE (not*
527 *shown), which was expected because of the dependence of MEE on particle size.* In contrast, the
528 values of *g* appear to differ only little between the sampled plumes for a given aerosol class. We
529 found *g* in the range of 0.67–0.76 for dust, 0.65–0.68 for biomass burning and 0.59–0.64 for
530 anthropogenic polluted aerosols at 550 nm. *g* values in dust plumes were high, which is expected
531 due to the presence of coarse particles contributing to forward scattering.

532

533 This analysis includes sampled aerosols originating from different source regions and having
534 undergone different aging and mixing processes, which could explain some of the variability. The

535 impact of these factors on the magnitude and spectral dependence of optical parameters will be
536 investigated in the following section.

537

538 **4. Discussion**

539 **4.1. Contribution of local anthropogenic pollution on aerosol absorption properties**

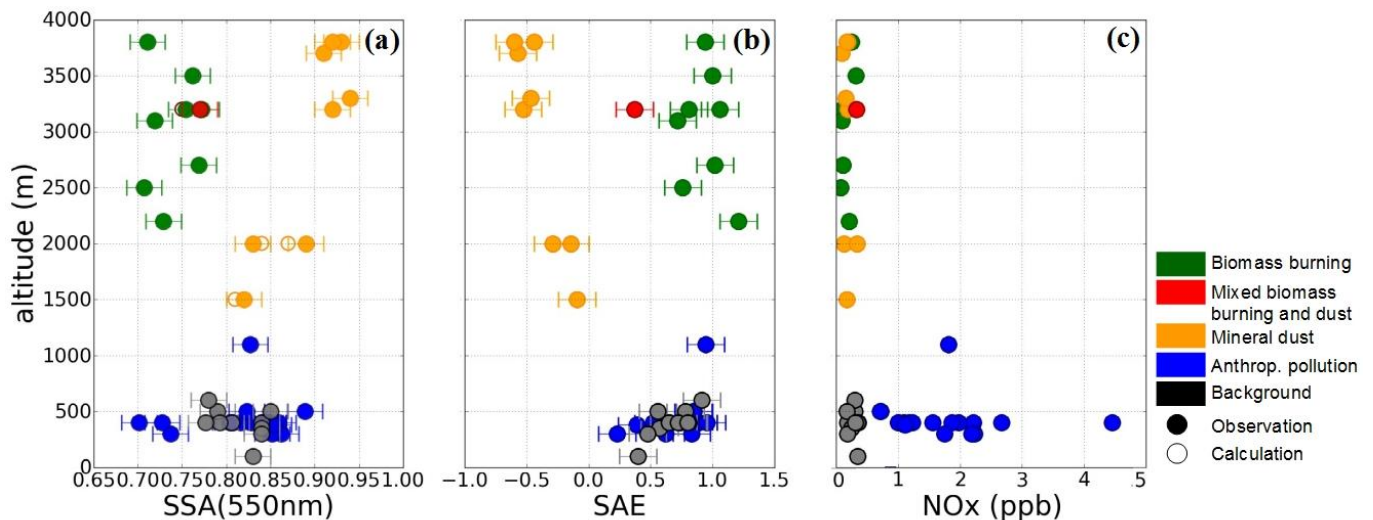
540 Figure 7 shows the vertical distribution of *SSA*, *SAE* and *NO_x* mixing ratio for the dominant
541 aerosol classification. ~~We exclusively consider measurements acquired during SLRs, since only~~
542 ~~during these phases the whole set of aerosol optical properties were measured.~~ In dust plumes, if
543 we exclude the case of mixing with biomass burning aerosol, *SSAs* were fairly constant above 2.5
544 km amsl with values ranging between 0.90 and 0.93 at 550 nm, in agreement with values reported
545 over dust source regions (*Schladitz et al., 2009; Formenti et al., 2011; Ryder et al., 2013, 2018*).
546 Despite the range of sources identified during DACCIWA, dust absorption properties do not seem
547 to be clearly linked to particle origin or time of transport. Aerosols were more absorbing within the
548 low-altitude dust plumes with *SSA* values dropping to 0.81. *SAE* values exhibited simultaneously a
549 sharp increase close to zero below 2.5 km amsl. This is consistent with a higher concentration of
550 fine particles, though the value of *SAE* was still much lower than for pollution or background
551 aerosol (i.e. where it is typically > 0.2), which means that scattering was still dominated by larger
552 particles. ~~The decrease in *NO_x* with height further indicates the concurrent influence by emissions~~
553 ~~from pollution sources in the low-altitude dust plumes.~~ Based on these observations, the strong
554 variation in the light-absorption properties of dust-dominated aerosol over SWA could be
555 attributed to the degree of mixing into the vertical column with either freshly emitted aerosols
556 from urban/industrial sources or long-range transported biomass burning aerosol.

557

558 One of the critical factors in the calculation of aerosol direct and semi-direct radiative effects is the
559 mixing state of the aerosols, which can significantly affect absorbing properties. There were no
560 direct observational constraints available on this property during the DACCIWA airborne
561 campaign. However, we investigated the probable aerosol mixing state by calculating composite
562 *SSA* from the aerosol size distribution. On the basis of Figure 5, dust size distribution showed only
563 minor discrepancies in the mean and standard deviation of the coarse mode but significant
564 differences in the balance between fine and coarse modes, which suggests low internal mixing of
565 dust with other atmospheric species. The size distributions of mixed dust-pollution have been
566 deconvoluted by weighting the size distributions of mineral dust and anthropogenic pollution
567 aerosol averaged over the respective flights. This assumes that dust was externally mixed with the
568 anthropogenic pollution particles and assumes a homogeneous size distribution for the dust and

569 anthropogenic pollution aerosol throughout a flight. σ_{scat} and σ_{abs} were then calculated using Mie
 570 theory from each composite size distributions and the corresponding k and m . The refractive
 571 indices at 550 nm were assumed to be 1.52-0.002i and 1.60-0.040i for dust and anthropogenic
 572 pollution particles, respectively, which are the mean values deduced from the data inversion
 573 procedure (i.e. section 2.3.1) throughout the campaign. The resulting σ_{scat} and σ_{abs} were used to
 574 calculate a composite SSA. A similar calculation was performed for the mixed dust-biomass
 575 burning case. Figure 7 shows a good agreement with the observations of SSA, implying that
 576 external mixing appears to be a reasonable assumption to compute aerosol direct and semi-direct
 577 radiative effects in these dust layers for modeling applications. This is consistent with the filter
 578 analysis performed during AMMA and SAMUM-2, which did not reveal any evidence of internal
 579 mixing in both mixed dust-biomass burning and dust-anthropogenic pollution layers (Chou *et al.*,
 580 2008; Lieke *et al.*, 2011; Petzold *et al.*, 2011).

581



582 **Figure 7. Vertical distribution of (a) the single scattering albedo at 550 nm, (b) the scattering**
 583 **Ångström exponent and (c) NOx mixing ratio for the dominant aerosol classification. In**
 584 **panel (a), full circles represent SSA measurements and empty circles represent composite**
 585 **SSA calculated by deconvoluting size distribution measurements in mixed dust layers and**
 586 **assuming an external mixing state.**

587
 588 ~~Figure 7 indicates markedly different processes affecting optical properties of biomass burning~~
 589 ~~aerosols.~~ SSA, SAE and NOx of biomass burning plumes did not significantly vary with height
 590 from 2.2 to 3.8 km amsl. Moreover, the size distribution of biomass burning aerosols for the
 591 observed cases did not show significant contribution of ultrafine particles (Figure 5). These
 592 observations seem to indicate that the absorption properties of biomass burning plumes were not
 593 affected by direct pollution emissions, ~~probably due to the remote location of the sampled biomass~~

594 ~~burning plumes as discussed in section 3.2. The optical properties of aerosols are determined by~~
595 ~~either the aerosol chemical composition, the aerosol size distribution, or both. Changes in the size~~
596 ~~distribution of biomass burning aerosol due to coagulation and condensation have been shown to~~
597 ~~alter the SSA, as particles increase towards sizes for which scattering is more efficient (Laing et al.,~~
598 ~~2016). Variations in particle chemical composition, caused by source emissions and aging~~
599 ~~processes associated with gas to particle transformation and internal mixing, has been shown to~~
600 ~~change the SSA (Abel et al., 2003; Petzold et al., 2011).~~

601

602 In the boundary layer, the similar SSA and SAE in anthropogenic pollution and background plumes
603 suggests that background aerosol may be rather called background pollution originating from a
604 regional background source in the far field. Our analysis of the spectral dependence of SSA
605 showed no apparent signature of anthropogenic pollution aerosols (see section 3.3) despite a strong
606 increase of aerosol number concentrations in air masses crossing urban centers (see section 3.2).
607 This can be explained by two factors: First, the majority of accumulation mode particles were
608 present in the background, while the large proportion of aerosols emitted from cities resided in the
609 ultrafine mode particles that have less scattering efficiencies (Figure 5). Second, large amounts of
610 absorbing aerosols in the background can minimize the impact of further increase of absorbing
611 particles to the aerosol load. ~~We did not find any correlation between the values of SSA and their~~
612 ~~spectral dependence, which suggests that the variability in SSA cannot be attributed to different~~
613 ~~contributions of marine aerosol in pollution plumes.~~ The high CO values (~180 ppb) observed in
614 background conditions further indicates a strong contribution of combustion emissions at the
615 surface. Recent studies showed a large background of biomass burning transported from the
616 Southern Hemisphere in SWA that dominated the aerosol chemical composition in the boundary
617 layer (Menuet et al., 2018; Haslett et al., 2019). ~~The high absorbing properties (SSA~0.81 at~~
618 ~~550nm) and the presence of particles both in the accumulation and super-micron modes (i.e.~~
619 ~~section 3.2.) in background plumes are consistent with being a mixture of aged absorbing biomass~~
620 ~~burning and Atlantic marine aerosol. Moreover SSA of background aerosol was lower than~~
621 ~~previously reported over the Southern Atlantic (Ascension Island) outside the fire season in~~
622 ~~Central Africa (Zuidema et al., 2018), which supports this conclusion.~~ These results highlight that
623 aerosol optical properties at the surface were dominated by the widespread biomass burning
624 particles at regional scale.

625

626 **4.2. Aging as a driver for absorption enhancement of biomass burning aerosol**

627 The optical properties of aerosols are determined by either the aerosol chemical composition, the
628 aerosol size distribution, or both. Changes in the size distribution of biomass burning aerosol due
629 to coagulation and condensation have been shown to alter the *SSA*, as particles increase towards
630 sizes for which scattering is more efficient (Laing *et al.*, 2016). Variations in particle chemical
631 composition, caused by source emissions and aging processes associated with gas-to-particle
632 transformation and internal mixing, has been shown to change the *SSA* (Abel *et al.*, 2003; Petzold
633 *et al.*, 2011).

634

635 In order to determine the contributions from size distribution and chemical composition to the
636 variation of *SSA* in biomass burning plumes, *SSA* is presented as a function of *SAE* and *k* in Figure
637 7a and b, respectively. *k* was iteratively varied to reproduce the experimental scattering and
638 absorption coefficients, as described in section 2.3.1. It appears that the variation of the size
639 distribution (assessed via *SAE* in Figure 8a) had minimal impact in determining the variability of
640 *SSA*. Thus, the observations suggest that there was no effect of plume age on the size distribution,
641 consistent with previous observations of size distribution in aged North American biomass
642 burning plumes (Sakamoto *et al.*, 2015; Carrico *et al.*, 2016; Laing *et al.*, 2016). Using a
643 Lagrangian microphysical model, Sakamoto *et al.* (2015) have shown a rapid shift to larger sizes
644 for biomass burning plumes within the first hours of aging. Less drastic but similarly rapid growth
645 by coagulation was seen by Capes *et al.* (2008) in their box model. Given that the biomass burning
646 plumes sampled during DACCIWA had more than 5 days in age, the quick size-distribution
647 evolution within the early plume stages might explain the limited impact of the size distribution on
648 the *SSA*.

649

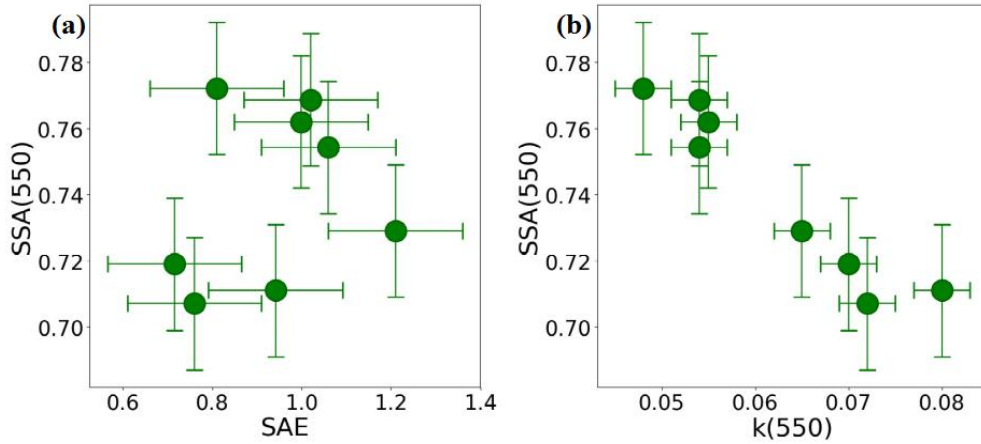


Figure 8. Contribution to single scattering albedo (a) from particle size (assessed via *SAE*) and (b) from composition (assessed via *k*) in biomass burning plumes.

650
651
652

653 In contrast, Figure 8b shows that there was a consistent decrease in *SSA* with increasing *k*,
 654 although there is some variability between the results from different plumes. The observed
 655 variability of *SSA* is reflected in a large variability of *k*, which is estimated to span the large range
 656 0.048–0.080 at 550 nm. *k* depends both on the aerosol chemical composition and size distribution
 657 (*Mita and Isono, 1980*). Given that *SSA* was found to be independent of the aerosol size
 658 distribution (Figure 8a), Figure 8b suggests that *SSA* variability was strongly influenced by the
 659 variability in composition of biomass burning aerosol, implying a high contribution for light-
 660 absorbing particles. ~~Although there is some variability between the results from different plumes,~~
 661 ~~overall there was a consistent decrease in *SSA* with increasing *k*, implying a high contribution for~~
 662 ~~light absorbing particles. The observed variability of *SSA* is reflected in a large variability of *k*,~~
 663 ~~which is estimated to span in the large range 0.048–0.080 at 550 nm.~~ No clear tendency was found
 664 for the wavelength dependence of *k*, which in some of the cases increases with wavelength and in
 665 others decreases (not shown). Correspondingly, values of *AAE* in biomass burning plumes ranged
 666 from 0.9 to 1.1 with a median value of 1.0. Theoretically, fine-mode aerosol with absorption
 667 determined exclusively by BC would have *AAE* equal to 1.0, since BC is expected to have a
 668 spectrally constant *k* (*Bond et al., 2013*). Therefore, the low *SSA* values observed in biomass
 669 burning plumes over SWA and the small spectral variation of *k* both suggest that BC is the
 670 dominant absorber in the visible and near-IR wavelengths for these biomass burning aerosols.

671

672 Compared with past in-situ measurements of aged biomass burning aerosol, *SSA* values over SWA
 673 (0.71–0.77 at 550 nm) are at the lower end of those reported worldwide (0.73–0.99 at 550 nm)
 674 (*Maggi et al., 2003; Reid et al. 2005; Johnson et al., 2008; Corr et al. 2012; Laing et al. 2016*).

675 This can be attributed in part to the high flaming versus smoldering conditions of African smoke
676 producing more BC particles (*Andreae and Merlet, 2001; Reid et al., 2005*), which inherently have
677 low SSA compared to other regions (*Dubovick et al. 2002*). However, SSA values over SWA are
678 significantly lower than the range reported near emission sources in sub-Saharan Africa and over
679 the southeast Atlantic, where values span over 0.84–0.90 at 550 nm (*Haywood et al., 2003b;*
680 *Pistone et al., 2019*). Recent observations carried out on Ascension Island to the south-west of the
681 DACCIIWA region showed that smoke transported from Central and South African fires can be
682 very light absorbing over the July-November burning season but SSA values were still higher
683 (0.80 ± 0.02 at 530 nm; *Zuidema et al., 2018*) than those reported over SWA. A possible cause of
684 the lower SSA in SWA is that Ascension Island is much closer to the local sources and the aerosol
685 is therefore less aged.

686

687 Currently there are few field measurements of well-aged biomass burning emissions. Our
688 knowledge of biomass burning aerosol primarily comes from laboratory experiments and near-
689 field measurements taken within a few hours of a wildfire (*Abel et al., 2003; Yokelson et al., 2009;*
690 *Adler et al., 2011; Haywood et al., 2003b; Vakkari et al., 2014; Zhong and Jang, 2014; Forrister*
691 *et al., 2015; Laing et al., 2016; Zuidema et al., 2018*). Exception made of the study by *Zuidema et*
692 *al. (2018)* over the southeast Atlantic, it is generally found that the aged biomass burning aerosol
693 particles are less absorbing than freshly emitted aerosols due to a combination of condensation of
694 secondary organic species and an additional increase in size by coagulation. This is in contrast to
695 our results showing that SSA of biomass burning aerosols were significantly lower than directly
696 after emission and that the evolution of SSA occurred long time after emission.

697

698 There are three possible explanations for these results. First, one must consider sample bias. As
699 regional smoke ages, it can be enriched by smoke from other fires that can smolder for days
700 producing large quantities of non-absorbing particles, thereby increasing the mean SSA (*Reid et al.,*
701 *2005; Laing et al., 2016*). However, during DACCIIWA, biomass burning plumes were transported
702 over the Atlantic Ocean and were probably less influenced by multiple fire emissions. Second,
703 there is evidence that fresh BC particles become coated with sulfate and organic species as the
704 plume ages in a manner that enhances their light absorption (*Lack et al., 2012; Schwarz et al.,*
705 *2008*). Finally, organic particles produced during the combustion phase can be lost during the
706 transport through photobleaching, volatilization and/or cloud-phase reactions (*Clarke et al., 2007;*
707 *Lewis et al., 2008; Forrister et al., 2015*), which is consistent with the low SSA and AAE values we
708 observed. Assessing whether these aging processes impact the chemical components and

709 henceforth optical properties of transported biomass burning aerosol would need extensive
710 investigation of aerosol chemical composition that will be carried out in a subsequent paper.

711

712 **5. Conclusions**

713 This paper provides an overview of *in-situ* airborne measurements of vertically resolved aerosol
714 optical properties carried out over SWA during the DACCIWA field campaign in June-July 2016.

715 The peculiar dynamics of the region lead to a chemically complex situation, which enabled
716 sampling various air masses, including long-range transport of biomass burning from Central
717 Africa and dust from Sahelian and Saharan sources, local anthropogenic plumes from the major
718 coastal cities, and mixtures of these different plumes. This work fills a research gap by providing,
719 firstly, key climate relevant aerosol properties (*SSA*, *MEE*, *g*, *SAE*, *AAE*) and secondly,
720 observations of the impact of aging and mixing processes on aerosols optical properties.

721

722 The aerosol vertical structure was very variable and mostly influenced by the origin of air mass
723 trajectories. While aerosol extinction coefficients generally decreased with height, there were
724 distinct patterns of profiles during dust and biomass burning transport to SWA. When present,
725 enhanced values of extinction coefficient up to 240 Mm^{-1} were observed in the 2–5 km amsl range.
726 These elevated aerosol layers were dominated by either dust or biomass burning aerosols, which is
727 consistent with what would be expected on the basis of the atmospheric circulations during the
728 monsoon season (*McConnell et al., 2008; Knippertz et al., 2017*). However, during one flight a
729 mixture of dust and biomass burning was found in a layer at around 3 km amsl, implying that there
730 may be substantial variability in the idealized picture. In the lower troposphere, the large
731 anthropogenic pollution plumes extended as far as hundreds of kilometers from the cities emission
732 sources and were not limited to the boundary layer but occurred also at higher levels up to 2.5 km
733 amsl, which is explained by vertical transport and mixing processes, partly triggered by the
734 orography of SWA (*Deroubaix et al., 2019; Flamant et al., 2018a*). The analysis of the aerosol size
735 distributions, *SAE* and *NOx* suggests a strong mixing of dust with anthropogenic pollution
736 particles in dust layers transported below 2.5 km amsl, whereas biomass burning plumes that were
737 transported more northward were not affected by this mixing. Both transport pathways and vertical
738 structures of biomass burning and dust plumes over SWA appear to be the main factors affecting
739 the mixing of anthropogenic pollution with dust and biomass burning particles.

740

741 The aerosol light absorption in dust plumes was strongly enhanced as the result of this mixing. We
742 find a decrease of *SSA(550nm)* from 0.92 to 0.81 for dust affected by anthropogenic pollution

743 mixing compared to the situation in which the dust plumes moved at higher altitudes across SWA.
744 Comparison of the particle size distributions of the different dust plumes showed a large
745 contribution of externally mixed fine mode particles in mixed layers, while there was no evidence
746 for internal mixing of coarse particles. Concurrent optical calculations by deconvoluting size
747 distribution measurements in mixed layers and assuming an external mixing state allowed to
748 reproduce the observed SSAs. This implies that an external mixing would be a reasonable
749 assumption to compute aerosol direct and semi-direct radiative effects in mixed dust layers.

750

751 Despite a strong increase of aerosol number concentration in air masses crossing urban
752 conglomerations, the magnitude of the spectral SSAs was comparable to the background.
753 Enhancements of light absorption properties were seen in some pollution plumes, but were not
754 statistically significant. A persistent spectral signature of biomass burning aerosols in both
755 background and pollution plumes highlights that the aerosol optical properties in the boundary
756 layer were strongly affected by the ubiquitous biomass burning aerosols transported from Central
757 Africa (*Menut et al., 2018; Haslett et al., 2019*). The large proportion of aerosols emitted from the
758 cities of Lomé, Accra and Abidjan that resided in the ultrafine mode particles have limited impact
759 on already elevated amounts of accumulation mode particles having a maximal absorption
760 efficiency. As a result, in the boundary layer, the contribution from local city emissions to aerosol
761 optical properties were of secondary importance at regional scale compared with this large
762 absorbing aerosol mass. While local anthropogenic emissions are expected to rise as SWA is
763 currently experiencing major economic and population growth, there is increasing evidence that
764 climate change is increasing the frequency and distribution of fire events (*Joly et al., 2015*). In
765 terms of future climate scenarios and accompanying aerosol radiative forcing, whether the large
766 biomass burning events that occur during the monsoon season would limit the radiative impact of
767 increasing anthropogenic emissions, remains an open and important question.

768

769 The SSA values of biomass burning aerosols transported in the free troposphere were very low
770 (0.71–0.77 at 550 nm) and have only rarely been observed in the atmosphere. The variability in
771 SSA was mainly controlled by the variability in aerosol composition (assessed via k) rather than by
772 variations in the aerosol size distribution. Correspondingly, values of AAE ranged from 0.9 to 1.1,
773 suggesting that BC particles were the dominant absorber in the visible for these biomass burning
774 aerosols. In recent years the southern Atlantic Ocean, especially the area of the west coast of
775 Africa, became an increasing focus in the research community, through the ORACLES/LASIC

776 (ObseRvations of Aerosols above CLouds and their intEractionS/Layered Atlantic Smoke
777 Interactions with Clouds), AEROCLO-sA (AErosol RadiatiOn and CLOuds in Southern Africa –
778 AEROCLO-SA) and CLARIFY (Cloud and Aerosols Radiative Impact and Forcing) projects
779 (*Zuidema et al.; 2016; Zuidema et al.; 2018; Formenti et al.; 2019*). Comparison with literature
780 showed a consistent picture of increasing absorption enhancement of biomass burning aerosol
781 from emission to remote locations. Further, the range of *SSA* values over SWA was slightly lower
782 than that reported on Ascension Island to the south-west of the DACCIWA region, which
783 underscores that the evolution of *SSA* occurred long time after emission. While the mechanism
784 responsible for this phenomenon warrants further study, our results support the growing body of
785 evidence that the optical parameters used in regional/global climate modeling studies, especially
786 absorption by biomass burning aerosols, have to be better constrained using these recent
787 observations to determine the direct and semi-direct radiative effects of smoke particles over this
788 region (*Mallet et al. 2019*). In particular and regarding the very high absorbing properties of
789 smoke, specific attention should be dedicated to the semi-direct effect of biomass burning aerosols
790 at the regional scale and its relative contribution to the indirect radiative effect.

791

792 We believe the set of DACCIWA observations presented here is representative of the regional
793 mean and variability in aerosol optical properties that can be observed during the monsoon season
794 over SWA, as the main dynamical features were in line with climatology (*Knippertz et al., 2017*).
795 This is why results from the present study will serve as input and constraints for climate modeling
796 to better understand the impact of aerosol particles on the radiative balance and cloud properties
797 over this region and also will substantially support remote sensing retrievals.

798 *Data availability.*

799 All data used in this study are publicly available on the AERIS Data and Service Center, which can
800 be found at <http://baobab.sedoo.fr/DACCIWA>.

801

802 *Author contributions.*

803 CD conducted the analysis of the data and wrote the paper. CD, TB, FB, NM, AC, PD, JB, RD, KS
804 and AS operated aircraft instruments and processed and/or quality-controlled data. MM provided
805 expertise on aerosol-climate interaction processes. CF and PK were PIs, who led the funding
806 application and coordinated the DACCIWA field campaign. All co-authors contributed to the
807 writing of the paper.

808

809 *Acknowledgements.*

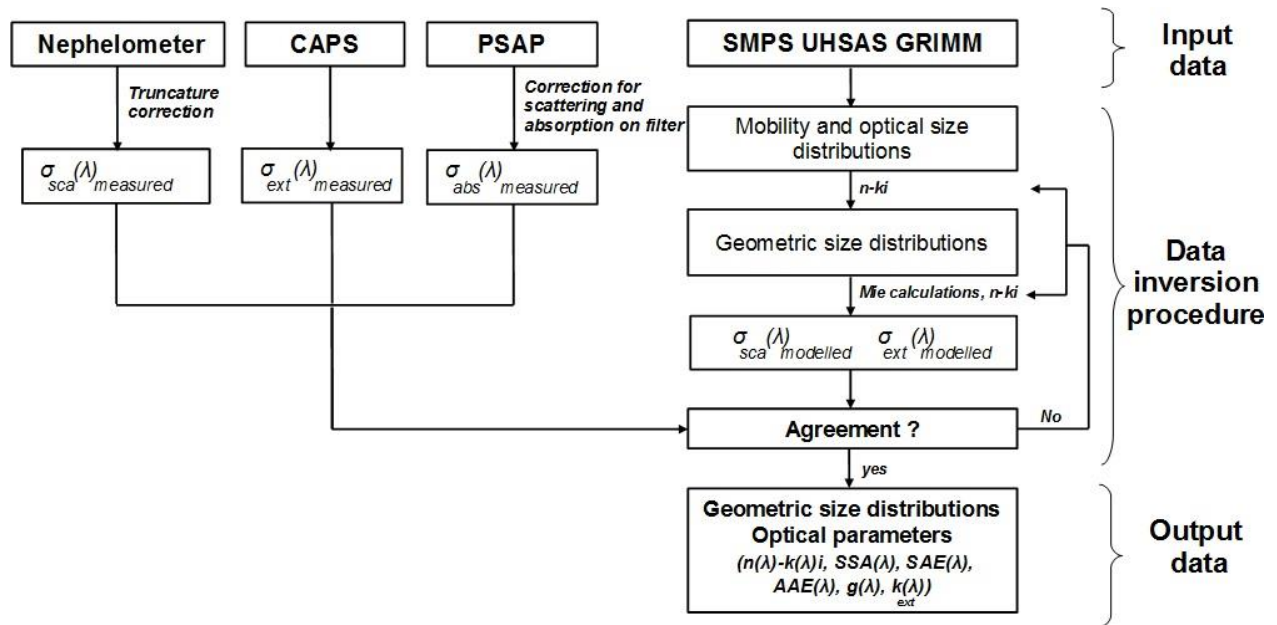
810 The research leading to these results has received funding from the European Union 7th
811 Framework Programme (FP7/2007-2013) under Grant Agreement no. 603502 (EU project
812 DACCIWA: Dynamics-aerosol-chemistry-cloud interactions in West Africa). The European
813 Facility for Airborne Research (EUFAR, <http://www.eufar.net/>) also supported the project through
814 the funding of the Transnational Activity project OLAETA and MICWA. We thank the Service des
815 Avions Français Instrumentés pour la Recherche en Environnement (SAFIRE, a joint entity of
816 CNRS, Météo-France, and CNES) and operator of the ATR-42 for their support during the aircraft
817 campaign. Cyrielle Denjean thanks CNES for financial support. The authors would like to thank
818 Bruno Piguet (CNRM) and Michel Ramonet (LSCE) for their support in the data processing.

819 **Appendix 1. Summary of flight information. All flights were conducted during 2016.**

Flight number	Date	Take off time (UTC)	Landing time (UTC)	Events observed
F17	29 June	14:17	17:10	Export of pollution from Lomé
F18	30 June	12:52	16:29	Export of pollution from Lomé
F19	1 July	10:35	14:06	Export of pollution from Accra
F20	2 July	09:53	13:21	Export of pollution from Lomé Dust outbreak
F21	2 July	15:04	18:29	Export of pollution from Lomé Biomass burning outbreak Mixed dust-biomass burning outbreak
F22	3 July	09:54	13:29	Export of pollution from Lomé
F24	6 July	07:17	11:03	Export of pollution from Abidjan
F27	8 July	05:52	09:28	Export of pollution from Accra
F28	8 July	10:53	14:22	Dust outbreak
F29	10 July	10:31	14:11	Export of pollution from Lomé Dust outbreak
F30	11 July	07:19	11:01	Export of pollution from Abidjan Biomass burning outbreak
F31	11 July	13:48	16:42	Biomass burning outbreak
F32	12 July	13:56	17:20	Export of pollution from Accra
F33	13 July	12:40	16:11	Biomass burning outbreak
F35	15 July	09:32	13:00	Export of pollution from Lomé

820

821 **Appendix 2. Data inversion procedure to calculate the aerosol microphysical and optical**
 822 **parameters.**



823

824 **References**

- 825 Abel, S. J., Haywood, J. M., Highwood, E. J., Li, J., and Buseck, P. R.: Evolution of biomass
826 burning aerosol properties from agricultural fire in southern Africa, *Geophys. Res. Lett.*, 30,
827 1783, doi:10.1029/2002GL017342, 2003.
- 828 Adler, G., Flores, J. M., Abo Riziq, A., Borrmann, S., and Rudich, Y., Chemical, physical, and
829 optical evolution of biomass burning aerosols: a case study, *Atmos. Chem. Phys.*, 11, 1491-
830 1503, <https://doi.org/10.5194/acp-11-1491-2011>, 2011.
- 831 Andreae, M.O. and Merlet, P., Emission of Trace Gases and Aerosols from Biomass Burning.
832 *Global Biogeochemical Cycles*, 15, 955-966, 2001.
- 833 Ansmann, A., Petzold, A., Kandler, K., Tegen, I. N. A., Wendisch, M., Müller, D., Weinzierl, B.,
834 Müller, T., and Heintzenberg, J.: Saharan Mineral Dust Experiments SAMUM-1 and
835 SAMUM-2: what have we learned?, *Tellus B*, 63, 403-429, doi: 10.1111/j.1600-
836 0889.2011.00555.x, 2011.
- 837 Bond, T. C., Doherty, S. J., Fahey, D. W., Forster, P. M., Berntsen, T., DeAngelo, B. J., Flanner, M.
838 G., Ghan, S., Kärcher, B., Koch, D., Kinne, S., Kondo, Y., Quinn, P. K., Sarofim, M. C.,
839 Schultz, M. G., Schulz, M., Venkataraman, C., Zhang, H., Zhang, S., Bellouin, N., Guttikunda, S.
840 K., Hopke, P. K., Jacobson, M. Z., Kaiser, J. W., Klimont, Z., Lohmann, U., Schwarz, J. P.,
841 Shindell, D., Storelvmo, T., Warren, S. G., and Zender, C. S.: Bounding the role of black carbon
842 in the climate system: A scientific assessment, *J. Geophys. Res.*, 118, 1-173,
843 doi:10.1002/jgrd.50171, 2013.
- 844 Boucher, O., D. Randall, P. Artaxo, C. Bretherton, G. Feingold, P. Forster, V.-M. Kerminen, Y.
845 Kondo, H. Liao, U. Lohmann, P. Rasch, S.K. Satheesh, S. Sherwood, B. Stevens, and X.Y.
846 Zhang: Clouds and aerosols. In *Climate Change 2013: The Physical Science Basis*.
847 Contribution of Working Group I to the Fifth Assessment Report of the Intergovernmental
848 Panel on Climate Change. T.F. Stocker, D. Qin, G.-K. Plattner, M. Tignor, S.K. Allen, J.
849 Doschung, A. Nauels, Y. Xia, V. Bex, and P.M. Midgley, Eds. Cambridge University Press, pp.
850 571-657, doi:10.1017/CBO9781107415324.016, 2013.
- 851 Capes, G., B. Johnson, G. McFiggans, P. I. Williams, J. M. Haywood, and H. Coe, Aging of
852 biomass burning aerosols over West Africa: Aircraft measurements of chemical composition,
853 microphysical properties and emission ratios, *J. Geophys. Res.*, 113, D00C15,
854 doi:10.1029/2008JD009845, 2008.
- 855 Carrico, C.M., Prenni, A.J., Kreidenweis, S.M., Levin, E.J., McCluskey, C.S., DeMott, P.J.,
856 McMeeking, G.R., Rapidly evolving ultrafine and fine mode biomass smoke physical

857 properties: comparing laboratory and field results, *J. Geophys. Res. Atmos.*, 121(10),
858 10.1002/2015JD024389, 2016.

859 Chen, G., Ziemba, L. D., Chu, D. A., Thornhill, K. L., Schuster, G. L., Winstead, E. L., Diskin, G.
860 S., Ferrare, R. A., Burton, S. P., Ismail, S., Kooi, S. A., Omar, A. H., Slusher, D. L., Kleb, M.
861 M., Reid, J. S., Twohy, C. H., Zhang, H., and Anderson, B. E.: Observations of Saharan dust
862 microphysical and optical properties from the Eastern Atlantic during NAMMA airborne field
863 campaign, *Atmos. Chem. Phys.*, 11, 723-740, <https://doi.org/10.5194/acp-11-723-2011>, 2011.

864 Chou, C., P. Formenti, M. Maille, P. Ausset, G. Helas, S. Osborne, and M. Harrison, Size
865 distribution, shape and composition of dust aerosols collected during the AMMA SOP0 field
866 campaign in the northeast of Niger, January 2006, *J. Geophys. Res.*, 113, D00C10,
867 doi:10.1029/2008JD009897, 2008.

868 Clarke, A., McNaughton, C., Kapustin, V., Shinozuka, Y., Howell, S., Dibb, J., Zhou, J., Anderson,
869 B., Brekhovskikh, V., Turner, H., and Pinkerton, M.: Biomass burning and pollution aerosol
870 over North America: organic components and their influence on spectral optical properties and
871 humidification response, *J. Geophys. Res.*, 112, D12S18, doi:10.1029/2006JD007777, 2007.

872 Corr, C. A., Hall, S. R., Ullmann, K., Anderson, B. E., Beyersdorf, A. J., Thornhill, K. L., Cubison,
873 M. J., Jimenez, J. L., Wisthaler, A., and Dibb, J. E.: Spectral absorption of biomass burning
874 aerosol determined from retrieved single scattering albedo during ARCTAS, *Atmos. Chem.*
875 *Phys.*, 12, 10505-10518, <https://doi.org/10.5194/acp-12-10505-2012>, 2012.

876 Deetz, K., Vogel, H., Haslett, S., Knippertz, P., Coe, H., and Vogel, B.: Aerosol liquid water
877 content in the moist southern West African monsoon layer and its radiative impact, *Atmos.*
878 *Chem. Phys.*, 18, 14271-14295, <https://doi.org/10.5194/acp-18-14271-2018>, 2018.

879 Denjean, C., Cassola, F., Mazzino, A., Triquet, S., Chevaillier, S., Grand, N., Bourriane, T.,
880 Momboisse, G., Sellegri, K., Schwarzenbock, A., Freney, E., Mallet, M., and Formenti, P.: Size
881 distribution and optical properties of mineral dust aerosols transported in the western
882 Mediterranean, *Atmos. Chem. Phys.*, 16, 1081-1104, <https://doi.org/10.5194/acp-16-1081-2016>,
883 2016.

884 Deroubaix, A., Menut, L., Flamant, C., Brito, J., Denjean, C., Dreiling, V., Fink, A., Jambert, C.,
885 Kalthoff, N., Knippertz, P., Ladkin, R., Mailler, S., Maranan, M., Pacifico, F., Pigué, B., Siour,
886 G., and Turquety, S.: Diurnal cycle of coastal anthropogenic pollutant transport over southern
887 West Africa during the DACCIWA campaign, *Atmos. Chem. Phys.*, 19, 473-497,
888 <https://doi.org/10.5194/acp-19-473-2019>, 2019.

889 Di Biagio, C., Formenti, P., Doppler, L., Gaimoz, C., Grand, N., Ancellet, G., Attié, J.-L., Bucci,
890 S., Dubuisson, P., Fierli, F., Mallet, M., and Ravetta, F.: Continental pollution in the Western

891 Mediterranean basin: large variability of the aerosol single scattering albedo and influence on
892 the direct shortwave radiative effect, *Atmos. Chem. Phys.*, 16, 10591-10607,
893 <https://doi.org/10.5194/acp-16-10591-2016>, 2016.

894 Dubovik, O., Holben, B. N., Eck, T. F., Smirnov, A., Kaufman, Y. J., King, M. D., Tanre, D., and
895 Slutsker, I.: Climatology of atmospheric aerosol absorption and optical properties in key
896 locations, *J. Atmos. Sci.*, 59, 590–608, 2002.

897 Flamant, C., Deroubaix, A., Chazette, P., Brito, J., Gaetani, M., Knippertz, P., Fink, A. H., de
898 Coetlogon, G., Menut, L., Colomb, A., Denjean, C., Meynadier, R., Rosenberg, P., Dupuy, R.,
899 Dominutti, P., Duplissy, J., Bourriane, T., Schwarzenboeck, A., Ramonet, M., and Totems, J.:
900 Aerosol distribution in the northern Gulf of Guinea: local anthropogenic sources, long-range
901 transport, and the role of coastal shallow circulations, *Atmospheric Chemistry and Physics*, 18,
902 12 363–12 389, <https://doi.org/10.5194/acp-18-12363-2018>, 2018a.

903 Flamant C., Knippertz, P., Fink, A. H., Akpo, A., Brooks, B., Chiu, C. J., Coe, H., Danuor, S.,
904 Evans, M., Jegede, O., Kalthoff, N., Konaré, A., Lioussé, C., Lohou, F., Mari, C., Schlager, H.,
905 Schwarzenboeck, A., Adler, B., Amekudzi, L., Aryee, J., Ayoola, M., Batenburg, A. M.,
906 Bessardon, G., Borrmann, S., Brito, J., Bower, K., Burnet, F., Catoire, V., Colomb, A., Denjean,
907 C., Fosu-Amankwah, K., Hill, P. G., Lee, J., Lathon, M., Maranan, M., Marsham, J.,
908 Meynadier, R., Ngamini, J.-B., Rosenberg, P., Sauer, D., Smith, V., Stratmann, G., Taylor, J. W.,
909 Voigt, C., and Yoboué, V.: The Dynamics-Aerosol-Chemistry-Cloud Interactions in West Africa
910 field campaign: Overview and research highlights, *B. Am. Meteorol. Soc.*, 99, 83–104,
911 <https://doi.org/10.1175/BAMS-D-16-0256.1>, 2018b.

912 Formenti, P., Rajot, J. L., Desboeufs, K., Saïd, F., Grand, N., Chevaillier, S., and Schmechtig, C.:
913 Airborne observations of mineral dust over western Africa in the summer Monsoons season:
914 spatial and vertical variability of physico-chemical and optical properties, *Atmos. Chem. Phys.*,
915 11, 6387–6410, [doi:10.5194/acp-11-6387-2011](https://doi.org/10.5194/acp-11-6387-2011), 2011.

916 Formenti, P., B. D’Anna, C. Flamant, M. Mallet, S.J. Piketh, K. Schepanski, F. Waquet, F. Auriol,
917 G. Brogniez, F. Burnet, J. Chaboureaud, A. Chauvigné, P. Chazette, C. Denjean, K. Desboeufs, J.
918 Doussin, N. Elguindi, S. Feuerstein, M. Gaetani, C. Giorio, D. Klopper, M.D. Mallet, P. Nabat,
919 A. Monod, F. Solmon, A. Namwoonde, C. Chikwililwa, R. Mushi, E.J. Welton, and B. Holben,
920 0: The Aerosols, Radiation and Clouds in southern Africa (AEROCLO-SA) field campaign in
921 Namibia: overview, illustrative observations and way forward. *Bull. Amer. Meteor. Soc.*, 0,
922 <https://doi.org/10.1175/BAMS-D-17-0278.1>, 2019.

923 Forrister, H., Liu, J., Scheuer, E., Dibb, J., Ziemba, L., Thornhill, K. L., Anderson, B., Diskin, G.,
924 Perring, A. E., and Schwarz, J. P.: Evolution of brown carbon in wildfire plumes, *Geophys.*
925 *Res. Lett.*, 42, 4623–4630, 2015.

926 Haslett, S. L., Taylor, J. W., Evans, M., Morris, E., Vogel, B., Dajuma, A., Brito, J., Batenburg, A.
927 M., Borrmann, S., Schneider, J., Schulz, C., Denjean, C., Bourriane, T., Knippertz, P., Dupuy,
928 R., Schwarzenböck, A., Sauer, D., Flamant, C., Dorsey, J., Crawford, I., and Coe, H.: Remote
929 biomass burning dominates southern West African air pollution during the monsoon, *Atmos.*
930 *Chem. Phys. Discuss.*, <https://doi.org/10.5194/acp-2019-38>, in review, 2019.

931 Haywood, J. M., Francis, P., Osborne, S., Glew, M., Loeb, N., Highwood, E., Tanre, D., Myhre, G.,
932 Formenti, P., and Hirst, E.: Radiative properties and direct radiative effect of Saharan dust
933 measured by the C-130 aircraft during SHADE:1. Solar spectrum, *J. Geophys. Res.-Atmos.*,
934 108, 8577, <https://doi.org/10.1029/2002jd002687>, 2003a.

935 Haywood, J. M., S. R. Osborne, P. N. Francis, A. Keil, P. Formenti, M. O. Andreae, and P. H. Kaye,
936 The mean physical and optical properties of regional haze dominated by biomass burning
937 aerosol measured from the C-130 aircraft during SAFARI 2000, *J. Geophys. Res.*, 108(D13),
938 8473, doi:10.1029/2002JD002226, 2003b.

939 Haywood, J. M., Pelon, J., Formenti, P., Bharmal, N., Brooks, M., et al.: Overview of the dust and
940 biomass-burning experiment and African Monsoon multidisciplinary analysis special observing
941 period-0., *J. Geophys. Res.*, 113, doi:10.1029/2008JD010077, 2008.

942 Heintzenberg, J., The SAMUM-1 experiment over Southern Morocco: Overview and introduction,
943 *Tellus Ser. B*, 61, 2-11, 2009.

944 Hess, M., Koepke, P., Schult I., Optical properties of aerosols and clouds, *Bull. Amer. Meteor.*
945 *Soc.*, 79, 831-844, 1998.

946 Janhäll, S., Andreae, M. O., and Pöschl, U.: Biomass burning aerosol emissions from vegetation
947 fires: particle number and mass emission factors and size distributions, *Atmos. Chem. Phys.*,
948 10, 1427-1439, <https://doi.org/10.5194/acp-10-1427-2010>, 2010.

949 Johnson, B. T., Heese, B., McFarlane, S. A., Chazette, P., Jones, A. et al.: Vertical distribution and
950 radiative effects of mineral dust and biomass burning aerosol over West Africa during DABEX,
951 *J. Geophys. Res.*, 113(D17), D00C12, doi:10.1029/2008JD009848, 2008.

952 Jolly, W. M., Cochrane, M. A., Freeborn, P. H., Holden, Z. A., Brown, T. J., Williamson, G. J., and
953 Bowman, D. M. J. S.: Climate-induced variations in global wild- fire danger from 1979 to
954 2013, *Nat. Commun.*, 6, 7537, <https://doi.org/10.1038/ncomms8537>, 2015.

955 Kalthoff, N., Lohou, F., Brooks, B., Jegede, G., Adler, B., Babić, K., Dione, C., Ajao, A.,
956 Amekudzi, L. K., Aryee, J. N. A., Ayoola, M., Bessardon, G., Danuor, S. K., Handwerker, J.,

957 Kohler, M., Lathon, M., Pedruzo-Bagazgoitia, X., Smith, V., Sunmonu, L., Wieser, A., Fink, A.
958 H., and Knippertz, P.: An overview of the diurnal cycle of the atmospheric boundary layer
959 during the West African monsoon season: results from the 2016 observational campaign,
960 *Atmos. Chem. Phys.*, 18, 2913-2928, <https://doi.org/10.5194/acp-18-2913-2018>, 2018.

961 Kirchstetter T. W. , Novakov, T., and Hobbs, P.: Evidence that the spectral dependence of light
962 absorption by aerosols is affected by organic carbon, *J. Geophys. Res.*, 109,
963 D21208,doi:10.1029/2004JD004999, 2004.

964 Knippertz, P., Evans, M. J., Field, P. R., Fink, A. H., Liousse, C., and Marsham, J. H.: The possible
965 role of local air pollution in climate change in West Africa, *Nat. Clim. Change*, 5, 815–822,
966 <https://doi.org/10.1038/nclimate2727>, 2015a.

967 Knippertz, P., Coe, H., Chiu, J. C., Evans, M. J., Fink, A. H., Kalthoff, N., Liousse, C., Mari, C.,
968 Allan, R. P., Brooks, B., Danour, S., Flamant, C., Jegede, O. O., Lohou, F., and Marsham, J. H.:
969 The dacciya project: Dynamics-Aerosol- Chemistry-Cloud Interactions in West Africa, *Bulletin*
970 *of the American Meteorological Society*, 96, 1451–1460, [https://doi.org/10.1175/BAMS-D-14-](https://doi.org/10.1175/BAMS-D-14-00108.1)
971 [00108.1](http://journals.ametsoc.org/doi/10.1175/BAMS-D-14-00108.1), <http://journals.ametsoc.org/doi/10.1175/BAMS-D-14-00108.1>, 2015b.

972 Knippertz, P., Fink, A. H., Deroubaix, A., Morris, E., Tocquer, F., Evans, M. J., Flamant, C.,
973 Gaetani, M., Lavaysse, C., Mari, C., Marsham, J. H., Meynadier, R., Affo-Dogo, A., Bahaga,
974 T., Brosse, F., Deetz, K., Guebsi, R., Latifou, I., Maranan, M., Rosenberg, 5 P. D., and
975 Schlueter, A.: A meteorological and chemical overview of the DACCIIWA field campaign in
976 West Africa in June-July 2016, *Atmospheric Chemistry and Physics*, 17, 10 893–10 918,
977 <https://www.atmos-chem-phys.net/17/10893/2017/>, 2017.

978 Lack, D. A. and Cappa, C. D.: Impact of brown and clear carbon on light absorption enhancement,
979 single scatter albedo and absorption wavelength dependence of black carbon, *Atmos. Chem.*
980 *Phys.*, 10, 4207–4220, doi:10.5194/acp-10-4207-2010, 2010.

981 Laing, J. R., Jaffe, D. A., and Hee, J. R.: Physical and optical properties of aged biomass burning
982 aerosol from wildfires in Siberia and the Western USA at the Mt. Bachelor Observatory, *Atmos.*
983 *Chem. Phys.*, 16, 15185-15197, <https://doi.org/10.5194/acp-16-15185-2016>, 2016.

984 Lebel, T., Parker, D.J., Flamant, C., Bourles, B., Marticorena, M., Mougín, E., Peugeot, C.,
985 Diedhiou, A., Haywood, J.M., Ngamini, J.B., Polcher, J., Redelsperger, J.L., Thorncroft, C.D.:
986 The AMMA field campaigns: multiscale and multidisciplinary observations in the West African
987 region, *Quarterly Journal of the Royal Meteorological Society*, 136(S1), 8–33, 2010.

988 Lewis, K., Arnott, W. P., Moosmuller, H., and Wold, C. E.: Strong spectral variation of biomass
989 smoke light absorption and single scattering albedo observed with a novel dual-wavelength
990 photoacoustic instrument, *J. Geophys. Res.*, 113, D16203, doi:10.1029/2007jd009699, 2008.

991 Lieke, K., Kandler, K., Scheuvens, D., Emmel, C., Von Glahn, C., Petzold, A., Weinzierl, B., Veira,
992 A., Ebert, M., Weinbruch, S., and SchÜTZ, L.: Particle chemical properties in the vertical
993 column based on aircraft observations in the vicinity of Cape Verde Islands, *Tellus B*, 63, 497-
994 511, doi: 10.1111/j.1600-0889.2011.00553.x, 2011.

995 Liousse, C., Assamoi, E., Criqui, P., Granier, C., and Rosset, R.: Explosive growth in African
996 combustion emissions from 2005 to 2030, *Environmental Research Letters*, 9, 035003,
997 <https://doi.org/10.1088/1748-9326/9/3/035003>, 2014.

998 Liu, D., Taylor, J. W., Crosier, J., Marsden, N., Bower, K. N., Lloyd, G., Ryder, C. L., Brooke, J.
999 K., Cotton, R., Marenco, F., Blyth, A., Cui, Z., Estelles, V., Gallagher, M., Coe, H., and
1000 Choulaton, T. W.: Aircraft and ground measurements of dust aerosols over the west African
1001 coast in summer 2015 during ICE-D and AER-D, *Atmos. Chem. Phys.*, 18, 3817-3838,
1002 <https://doi.org/10.5194/acp-18-3817-2018>, 2018.

1003 Magi, B. I., Magi A., Hobbs P.V., Schmid B., and Redemann J., Vertical profiles of light scattering,
1004 light absorption and single-scattering albedo during the dry, biomass burning season in
1005 southern Africa and comparisons of in situ and remote sensing measurements of aerosol optical
1006 depths, *Journal of Geophysical Research*, 108 (D13), doi:10.1029/2002JD002361, 2003.

1007 Mallet, M., Nabat, P., Zuidema, P., Redemann, J., Sayer, A. M., Stengel, M., Schmidt, S.,
1008 Cochrane, S., Burton, S., Ferrare, R., Meyer, K., Saide, P., Jethva, H., Torres, O., Wood, R.,
1009 Saint Martin, D., Roehrig, R., Hsu, C., and Formenti, P.: Simulation of the transport, vertical
1010 distribution, optical properties and radiative impact of smoke aerosols with the ALADIN
1011 regional climate model during the ORACLES-2016 and LASIC experiments, *Atmos. Chem.*
1012 *Phys.*, 19, 4963-4990, <https://doi.org/10.5194/acp-19-4963-2019>, 2019.

1013 Mann, G. W., Carslaw, K. S., Reddington, C. L., Pringle, K. J., Schulz, M., Asmi, A., Spracklen, D.
1014 V., Ridley, D. A., Woodhouse, M. T., Lee, L. A., Zhang, K., Ghan, S. J., Easter, R. C., Liu, X.,
1015 Stier, P., Lee, Y. H., Adams, P. J., Tost, H., Lelieveld, J., Bauer, S. E., Tsigaridis, K., van Noije,
1016 T. P. C., Strunk, A., Vignati, E., Bellouin, N., Dalvi, M., Johnson, C. E., Bergman, T., Kokkola,
1017 H., von Salzen, K., Yu, F., Luo, G., Petzold, A., Heintzenberg, J., Clarke, A., Ogren, J. A., Gras,
1018 J., Baltensperger, U., Kaminski, U., Jennings, S. G., O'Dowd, C. D., Harrison, R. M., Beddows,
1019 D. C. S., Kulmala, M., Viisanen, Y., Ulevicius, V., Mihalopoulos, N., Zdimal, V., Fiebig, M.,
1020 Hansson, H.-C., Swietlicki, E., and Henzing, J. S.: Intercomparison and evaluation of global
1021 aerosol microphysical properties among AeroCom models of a range of complexity, *Atmos.*
1022 *Chem. Phys.*, 14, 4679-4713, <https://doi.org/10.5194/acp-14-4679-2014>, 2014.

1023 Mari, C. H., Cailley, G., Corre, L., Saunois, M., Attié, J. L., Thouret, V., and Stohl, A.: Tracing
1024 biomass burning plumes from the Southern Hemisphere during the AMMA 2006 wet season

1025 experiment, *Atmos. Chem. Phys.*, 8, 3951-3961, <https://doi.org/10.5194/acp-8-3951-2008>,
1026 2008.

1027 Martinorena, B. and Bergametti, G.: Two-year simulations of seasonal and interannual changes of
1028 the Saharan dust emissions, *Geophys. Res. Lett.*, 23, 1921-1924, 1996.

1029 McConnell, C. L., Highwood, E. J., Coe, H., Formenti, P., Anderson, B., Osborne, S., Nava, S.,
1030 Desboeufs, K., Chen, G., and Harrison, M. A. J.: Seasonal variations of the physical and optical
1031 characteristics of Saharan dust: Results from the Dust Outflow and Deposition to the Ocean
1032 (DODO) experiment, *J. Geophys. Res.*, 113, D14S05, doi:10.1029/2007JD009606, 2008.

1033 McMeeking, G. R., Fortner, E., Onasch, T. B., Taylor, J. W. Flynn, M., Coe, H., and Kreidenweis,
1034 S. M.: Impacts of non-refractory material on light absorption by aerosols emitted from biomass
1035 burning, *J. Geophys. Res.-Atmos.*, 119, 2014JD021750,
1036 <https://doi.org/10.1002/2014JD021750>, 2014.

1037 Menut, L., Flamant, C., Turquety, S., Deroubaix, A., Chazette, P., and Meynadier, R.: Impact of
1038 biomass burning on pollutant surface concentrations in megacities of the Gulf of Guinea,
1039 *Atmospheric Chemistry and Physics*, 18, 2687–20 2707, [https://doi.org/10.5194/acp-18-2687-](https://doi.org/10.5194/acp-18-2687-2018)
1040 2018, 2018.

1041 Mertes, S., Schröder, F., Wiedensohler, A.: The particle detection efficiency curve of the TSI 3010
1042 CPC as a function of the temperature difference between saturator and condenser, *Aerosol*
1043 *Science and Technology*, 23, pp. 257-261, 1995.

1044 Mita, A., Isono, K., Effective complex refractive index of atmospheric aerosols containing
1045 absorbing substances, *J. Meteorol. Soc. Jpn.*, 58, 69-80,
1046 https://doi.org/10.2151/jmsj1965.58.1_69 1980.

1047 Myhre, G., Samset, B. H., Schulz, M., Balkanski, Y., Bauer, S., Berntsen, T. K., Bian, H., Bellouin,
1048 N., Chin, M., Diehl, T., Easter, R. C., Feichter, J., Ghan, S. J., Hauglustaine, D., Iversen, T.,
1049 Kinne, S., Kirkevåg, A., Lamarque, J.-F., Lin, G., Liu, X., Lund, M. T., Luo, G., Ma, X., van
1050 Noije, T., Penner, J. E., Rasch, P. J., Ruiz, A., Seland, Skeie, R. B., Stier, P., Takemura, T.,
1051 Tsigaridis, K., Wang, P., Wang, Z., Xu, L., Yu, H., Yu, F., Yoon, J.-H., Zhang, K., Zhang, H.,
1052 and Zhou, C.: Radiative forcing of the direct aerosol effect from AeroCom Phase II simulations,
1053 *Atmos. Chem. Phys.*, 13, 1853-1877, <https://doi.org/10.5194/acp-13-1853-2013>, 2013.

1054 Petzold, A., Rasp, K., Weinzierl, B., Esselborn, M., Hamburger, T., Dornbrack, A., Kandler, K.,
1055 Schutz, L., Knippertz, P., Fiebig, M., and Virkkula, A.: Saharan dust refractive index and optical
1056 properties from aircraft-based observations during SAMUM 2006, *Tellus B*, 61 118–130, 2009

1057 Petzold, A., Veira, A., Mund, S., Esselborn, M., Kiemle, C., Weinzierl, B., Hamburger, T., Ehret,
1058 G., Lieke, K., and Kandler, K.: Mixing of mineral dust with urban pollution aerosol over Dakar

1059 (Senegal): impact on dust physico-chemical and radiative properties, *Tellus B*, 63, 619-634,
1060 doi: 10.1111/j.1600-0889.2011.00547.x, 2011.

1061 Pistone, K., Redemann, J., Doherty, S., Zuidema, P., Burton, S., Cairns, B., Cochrane, S., Ferrare,
1062 R., Flynn, C., Freitag, S., Howell, S., Kacenelenbogen, M., LeBlanc, S., Liu, X., Schmidt, K.
1063 S., Sedlacek III, A. J., Segal-Rosenhaimer, M., Shinozuka, Y., Stamnes, S., van Dierenhoven,
1064 B., Van Harten, G., and Xu, F.: Intercomparison of biomass burning aerosol optical properties
1065 from in-situ and remote-sensing instruments in ORACLES-2016, *Atmos. Chem. Phys.*
1066 *Discuss.*, <https://doi.org/10.5194/acp-2019-142>, in review, 2019.

1067 Reid, J. S., Eck, T. F., Christopher, S. A., Koppmann, R., Dubovik, O., Eleuterio, D. P., Holben, B.
1068 N., Reid, E. A., and Zhang, J.: A review of biomass burning emissions part III: intensive optical
1069 properties of biomass burning particles, *Atmos. Chem. Phys.*, 5, 827–849, doi:10.5194/acp-5-
1070 827-2005, 2005.

1071 Roehrig, R., D. Bouniol, F. Guichard, F. D. Hourdin, and J. L. Redelsperger, The present and
1072 future of the west african monsoon: A process-oriented assessment of CMIP5 simulations along
1073 the AMMA transect, *J. Clim.*, 26, 6471–6505, doi:10.1175/JCLI-D-12-00505.1, 2013.

1074 Russell M., Zhang, S.-H., Flagan, R.C., Seinfeld, J.H., Stolzenburg, M.R., Caldow, R.: Radially
1075 classified aerosol detector for aircraft-based submicron aerosol measurements, *Journal of*
1076 *Atmospheric and Oceanic Technology*, 13, 598-609, 1996.

1077 Ryder, C. L., Highwood, E. J., Rosenberg, P. D., Trembath, J., Brooke, J. K., Bart, M., Dean, A.,
1078 Crosier, J., Dorsey, J., Brindley, H., Banks, J., Marsham, J. H., McQuaid, J. B., Sodemann, H.,
1079 and Washington, R.: Optical properties of Saharan dust aerosol and contribution from the
1080 coarse mode as measured during the Fennec 2011 aircraft campaign, *Atmos. Chem. Phys.*, 13,
1081 303–325, <https://doi.org/10.5194/acp-13-303-2013>, 2013.

1082 Ryder, C. L., Marengo, F., Brooke, J. K., Estelles, V., Cotton, R., Formenti, P., McQuaid, J. B.,
1083 Price, H. C., Liu, D., Ausset, P., Rosenberg, P. D., Taylor, J. W., Choularton, T., Bower, K., Coe,
1084 H., Gallagher, M., Crosier, J., Lloyd, G., Highwood, E. J., and Murray, B. J.: Coarse-mode
1085 mineral dust size distributions, composition and optical properties from AER-D aircraft
1086 measurements over the tropical eastern Atlantic, *Atmos. Chem. Phys.*, 18, 17225-17257,
1087 <https://doi.org/10.5194/acp-18-17225-2018>, 2018.

1088 Sakamoto, K. M., Allan, J. D., Coe, H., Taylor, J. W., Duck, T. J., and Pierce, J. R.: Aged boreal
1089 biomass-burning aerosol size distributions from BORTAS 2011, *Atmos. Chem. Phys.*, 15,
1090 1633–1646, doi:10.5194/acp-15-1633-2015, 2015.

1091 Sakamoto, K. M., Laing, J. R., Stevens, R. G., Jaffe, D. A., and Pierce, J. R.: The evolution of
1092 biomass-burning aerosol size distributions due to coagulation: dependence on fire and

1093 meteorological details and parameterization, *Atmos. Chem. Phys.*, 16, 7709-7724,
1094 <https://doi.org/10.5194/acp-16-7709-2016>, 2016.

1095 Schladitz, A., Muller, T., Kaaden, N., Massling, A., Kandler, K., Ebert, M., Weinbruch, S.,
1096 Deutscher, C., and Wiedensohler, A.: In situ measurements of optical properties at Tinfou
1097 (Morocco) during the Saharan Mineral Dust Experiment SAMUM 2006, *Tellus B*, 61, 64–78,
1098 doi:10.1111/j.1600-0889.2008.00397.x, 2009.

1099 Schuster, G. L., Dubovik, O., and Holben, B. N.: Angstrom exponent and bimodal aerosol size
1100 distributions, *J. Geophys. Res.*, 111, D07207, doi:10.1029/2005JD006328, 2006.

1101 Schwarz, J. P., et al., Coatings and their enhancement of black carbon light absorption in the
1102 tropical atmosphere, *J. Geophys. Res.*, 113, D03203, doi:10.1029/2007JD009042, 2008.

1103 Seinfeld, J. H. and Pandis, S. N.: Properties of the Atmospheric Aerosol, in: *Atmospheric*
1104 *Chemistry and Physics: From Air Pollution to Climate Change*, 2nd ed., John Wiley & Sons,
1105 New Jersey, USA, 350–388, 2006.

1106 Shin, S.-K., Tesche, M., Noh, Y., and Müller, D.: Aerosol-type classification based on AERONET
1107 version 3 inversion products, *Atmos. Meas. Tech.*, 12, 3789–3803, [https://doi.org/10.5194/amt-](https://doi.org/10.5194/amt-12-3789-2019)
1108 [12-3789-2019](https://doi.org/10.5194/amt-12-3789-2019), 2019.

1109 Silva, S. and Arellano, A.: Characterizing regional-scale combustion using satellite retrievals of
1110 CO, NO₂ and CO₂, *Remote Sensing*, 9, 744, <https://doi.org/10.3390/rs9070744>, 2017.

1111 Solmon, F., Mallet, M., Elguindi, N., Giorgi, F., Zakey, A., and Konare, A.: Dust aerosol impact on
1112 regional precipitation over western Africa, mechanisms and sensitivity to absorption properties,
1113 *Geophys. Res. Lett.*, 35, L24705, doi:10.1029/2008GL035900, 2008

1114 Stier, P., Schutgens, N. A. J., Bellouin, N., Bian, H., Boucher, O., Chin, M., Ghan, S., Huneeus, N.,
1115 Kinne, S., Lin, G., Ma, X., Myhre, G., Penner, J. E., Randles, C. A., Samset, B., Schulz, M.,
1116 Takemura, T., Yu, F., Yu, H., and Zhou, C.: Host model uncertainties in aerosol radiative
1117 forcing estimates: results from the AeroCom Prescribed intercomparison study, *Atmos. Chem.*
1118 *Phys.*, 13, 3245-3270, <https://doi.org/10.5194/acp-13-3245-2013>, 2013.

1119 Stohl, A., Eckhardt, S., Forster, C., James, P., Spichtinger, N., and Seibert, P.: A replacement for
1120 simple back trajectory calculations in the interpretation of atmospheric trace substance
1121 measurements, *Atmos. Environ.*, 36, 4635–4648, 2002.

1122 Vakkari, V., Kerminen, V. M., Beukes, J. P., Tiitta, P., van Zyl, P. G., Josipovic, M., Venter, A. D.,
1123 Jaars, K., Worsnop, D. R., Kulmala, M., and Laakso, L.: Rapid changes in biomass burning
1124 aerosols by atmospheric oxidation, *Geophys. Res. Lett.*, 41, 2644–2651,
1125 doi:10.1002/2014gl059396, 2014.

1126 Virkkula, A., Correction of the Calibration of the 3-wavelength Particle Soot Absorption
1127 Photometer (3λ PSAP), *Aerosol Science and Technology*, 44:8, 706-712, DOI:
1128 10.1080/02786826.2010.482110, 2010.

1129 Wang, T., T. F. Cheung, Y. S. Li, X. M. Yu, and D. R. Blake, Emission characteristics of CO, NO_x
1130 ,SO₂ and indications of biomass burning observed at a rural site in eastern China, *J. Geophys.*
1131 *Res.*, 107 (D12), 4157, doi:10.1029/2001JD000724, 2002.

1132 Weinzierl, B., Sauer, D., Esselborn, M., Petzold, A., Veira, A., Rose, M., Mund, S., Wirth, M.,
1133 Ansmann, A., Tesche, M., Gross, S., and Freudenthaler, V.: Microphysical and optical
1134 properties of dust and tropical biomass burning aerosol layers in the Cape Verde region—an
1135 overview of the airborne in situ and lidar measurements during SAMUM-2, *Tellus B*, 63, 589-
1136 618, doi: 10.1111/j.1600-0889.2011.00566.x, 2011.

1137 Wiedensohler, A., Orsini, D., Covert, D.S., Coffmann, D., Cantrell, W., Havlicek, M., Brechtel,
1138 F.J., Russell, L.M., Weber, R.J., Gras, J., Hudson, J.G., Litchy M.: Intercomparison study of
1139 size-dependent counting efficiency of 26 condensation particle counters, *Aerosol Science and*
1140 *Technology*, 27, 224-242, 1997.

1141 Yokelson, R. J., Crouse, J. D., DeCarlo, P. F., Karl, T., Urbanski, S., Atlas, E., Campos, T.,
1142 Shinzuka, Y., Kapustin, V., Clarke, A. D., Weinheimer, A., Knapp, D. J., Montzka, D. D.,
1143 Holloway, J., Weibring, P., Flocke, F., Zheng, W., Toohey, D., Wennberg, P. O., Wiedinmyer, C.,
1144 Mauldin, L., Fried, A., Richter, D., Walega, J., Jimenez, J. L., Adachi, K., Buseck, P. R., Hall,
1145 S. R., and Shetter, R.: Emissions from biomass burning in the Yucatan, *Atmos. Chem. Phys.*, 9,
1146 5785-5812, <https://doi.org/10.5194/acp-9-5785-2009>, 2009.

1147 Zhong, M. and Jang, M.: Dynamic light absorption of biomass-burning organic carbon
1148 photochemically aged under natural sunlight, *Atmos. Chem. Phys.*, 14, 1517-1525,
1149 <https://doi.org/10.5194/acp-14-1517-2014>, 2014.

1150 Zhai, J., Lu, X., Li, L., Zhang, Q., Zhang, C., Chen, H., Yang, X., and Chen, J.: Size-resolved
1151 chemical composition, effective density, and optical properties of biomass burning particles,
1152 *Atmos. Chem. Phys.*, 17, 7481-7493, <https://doi.org/10.5194/acp-17-7481-2017>, 2017.

1153 Zuidema, P., Redeman, J., Haywood, J., Wood, R., Piketh, S., Hipondoka, M. and Formenti, P.:
1154 Smoke and clouds above the southeast Atlantic: upcoming field campaigns probe absorbing
1155 aerosols impact on climate, *Bull. Am. Meteorol. Soc.*, doi: 10.1175/BAMS-D-15-00082.1,
1156 2016.

1157 Zuidema, P., Sedlacek III, A. J., Flynn, C., Springston, S., Delgadillo, R., Zhang, J., Aiken, A. C.,
1158 Koontz, A., Muradyan, P., and Zuidema, P.: The Ascension Island boundary layer in the remote

1159 southeast Atlantic is often smoky, *Geophysical Research Letters*, In Press, 4456–4465,
1160 <https://doi.org/10.1002/2017GL076926>, 2018.